CALORIMETRIC DETERMINATION OF THE HEATS OF RETORTING GREEN RIVER AND RUNDLE OIL SHALES TO 500°C AND OF THE HEAT OF COMBUSTION OF SPENT GREEN RIVER SHALE AT 705°C

Stephen C. Mraw and Charles F. Keweshan

Exxon Research and Engineering Co.
Clinton Township, Annandale, New Jersey 08801

INTRODUCTION

Two important considerations for the future production of oil from shale are solids handling and heat management. For a resource yielding about 90 ℓ/tonne†, two tonnes of rock must be handled for each barrel of oil produced, and large quantities of heat must be supplied or removed for the high-temperature processes involved. Proper reactor design and efficient process operations require accurate enthalpy data for retorting raw shale and combusting spent shale. It is part of our program in high-temperature calorimetry to develop novel techniques for oil-shale measurements and to provide accurate enthalpy data for shales of commercial interest. In previous papers, we have described a new method for determining the enthalpy of vaporization of organic materials at high temperatures (1), demonstrated the application of this method to oil-shale systems (2), and given a complete set of results for the heat of retorting raw Colorado Green River and Australian Rundle oil shales to 500°C (3). In the present paper we present new results for the heat of combustion of spent Green River shales at 705°C.

EXPERIMENTAL METHOD

Our apparatus is the high-temperature Calvet-type calorimeter described previously (4). Briefly, it consists of a central inconel block surrounded by a furnace designed for operation from room temperature to 1000°C. Within the block are two symmetrically mounted wells which serve as sample chambers. Each well is surrounded by a multi-junction thermopile which monitors the temperature difference between the well and the block. When any process within the sample chamber absorbs or liberates heat, the thermopile signal observed is proportional to the heat flow between the chamber and the block. The twin thermopiles are wired in opposition so that a difference reading is obtained for the left versus right sample chambers. A diagram of the apparatus is shown in Figure 1.

Most of the experiments to be described are "drop" experiments. A quartz or ceramic tube within the sample chamber is continuously swept with gas (nitrogen or oxygen, depending on the experiment), and a sample is dropped from room temperature into the receiving tube at the high temperature of the calorimeter. A peak in the thermopile signal records the total heat necessary to bring the sample from room temperature to its final state at high temperature. The area of the peak is directly proportional to the total heat.

---

† ℓ/tonne = 4.174 U.S. gal/ton

In the case of samples dropped into nitrogen, we have developed a novel method for determining the heat necessary for rapid vaporization processes in the calorimeter (1). When a sample of an organic compound, or of a complex mixture, is dropped into the calorimeter at a temperature where evaporation or boiling is rapid, all processes can be completed within the time constant of the calorimeter (about 2 to 3 minutes). The calorimeter thermopile then responds "ballistically", and the peak height (as well as the more traditional peak area) is directly proportional to the total heat transferred to the sample. In Reference 2 we showed that the method was accurate beyond pure compounds and could be used to determine the heats associated with oil-shale processes. Results on Green River oil shale for the total enthalpy change

$$\text{raw shale (25°C)} \rightarrow \text{spent shale} + \text{volatiles (500°C)} \qquad 1)$$

agreed very well with those from an earlier study using an entirely different technique (5).

In addition, this experiment for a complex material such as oil shale presents an opportunity to study the physical chemistry of the associated processes. When a sample is dropped into high temperature, some processes may be completed within the response time of the calorimeter, and other processes may take longer. The peak-height value will accurately represent the heat for the rapid processes, while the peak-area value will represent the total heat for all of the processes until the calorimeter returns to equilibrium (about 1.5 to 2.5 hours). Although comparison of the peak-height and peak-area values for each run nominally distinguishes rapid vs. slower processes, this can sometimes allow a distinction between organic and inorganic contributions. In Reference 3, we presented results for two complete sink-float series of raw shales, Colorado Green River and Australian Rundle. The enthalpy quantities for equation 1 were accurately determined, and the comparison of peak-height and peak-area values showed the importance of slower inorganic processes occurring in the Rundle shales at 500°C.

Calibration of the calorimetric sensitivity, both for endo- and exothermic events, is interspersed repeatedly among the actual shale experiments. For endothermic drops into nitrogen, the calorimetric sensitivity is determined by dropping samples of α-Al_2O_3 into the calorimeter and recording both the height and area of the resulting peak. From the known enthalpy change (6) of Al_2O_3 between room temperature and the calorimeter temperature, both a peak-height and a peak-area calibration constant are calculated. For exothermic combustion experiments, the calorimetric sensitivity is determined using a calibration heater wound onto the ceramic tube which serves as the gas delivery inlet. A heat pulse is generated using a precision power supply, and the total heat is calculated from the known voltage and the measured resistance.

OIL-SHALE SAMPLES

The raw Green River oil-shale samples are from the sink-float separation procedures developed at Exxon Research and Engineering Company in Baytown, Texas (7). They are the same as those used in our retorting studies (3) and are from the Mahogany Zone (Colony Mine), ranging from 87 to 340 ℓ/tonne (21 to 82 U.S. gal/ton) Fischer Assay. Compositional details, includ-

ing mineral analyses, have been given by Vadovic (7). The powdered shale samples were dried in our laboratory over a P_2O_5 desiccant to remove surface moisture and loosely held water. Occasional checks have indicated that this process removes an amount of water comparable to that removed by drying at 105°C.

COMBUSTION OF SPENT GREEN RIVER SHALE AT 705°C

Combustion of Model Carbonaceous Materials

The electrical calibration procedure outlined earlier determines the calibration constant for the relatively "sterile" procedure of a controlled electrical power input within the thermopile reaction zone. To determine whether this constant is applicable to a vigorously combusting organic sample at high temperature, we performed several chemical checks using model combustions.

At 750°C, we measured the heat of combustion of SP-1 graphite (8). In our first experiments, using dry oxygen, the heat of combustion values were widely scattered and invariably low with respect to the literature value for graphite (9). We suspected incomplete combustion of carbon monoxide, and, when we humidified the oxygen by bubbling it through liquid water at room temperature (10), the combustion values immediately improved to within 3 to 4 percent of the literature value. By adjusting the gas flow rate to change the residence time of gases in the reaction zone, we eventually obtained an accuracy of 1 to 2 percent. Thus, all subsequent combustions of shale samples used humidifed oxygen at a flow rate of 20 cm^3/min. Further tests, both at 705 and 750°C, were made by combusting the highly-porous amorphous carbon, spherocarb (11), to simulate the rapid burning of a spent shale sample, and these tests indicated that the electrical calibration constant, even when applied to a rapid combustion, gives the true enthalpy value within a few percent.

To test whether volatile materials would combust within the thermopile zone under our conditions, we dropped samples of heavy, pure aromatic compounds directly into the oxygen stream in the calorimeter at 705°C. We used 1,2,5,6-dibenzanthracene (t_{bp} = 524°C) and coronene (t_{bp} = 525°C), and sample sizes (about 2 to 3 mg) were chosen to simulate the amount of organic that might volatilize from a spent shale sample. Even though combustion was not complete (60 to 90 percent of the expected enthalpy), we concluded that, if our system was this efficient in combusting these refractory molecules, we could expect volatile materials evolving from a spent shale to be combusted as well.

Preparation of Spent Shales

Pellets of each raw shale were pyrolyzed in a thermogravimetric analyser (TGA) to 500°C at heating rates of 50 to 100°C/min and held for 20 minutes. Most of the pellets could be recovered intact from the TGA and used for subsequent experiments. For pellets of the two richest samples, however, there was considerable swelling and cracking, often causing mechanical loss of some of the material. These pellets had to be held in gold crucibles during the TGA runs and in subsequent calorimetry experiments. To check that the TGA purge gas was reasonably free of oxygen, occasional samples were

held at 500°C for periods of 40 minutes to four hours. There was no detectable mass change during these time periods. When the subsequent heat of combustion was compared to that of samples held for only 20 minutes, no loss of heating value was observed, indicating that no serious sample oxidation had occurred.

For each raw shale in the series, several pellets (approximately 30 to 100 mg each) were pyrolyzed in the TGA. Some were saved for calorimetric experiments, while, in general, two of each member of the series were sent for analysis (12). The resulting analyses are given in Table 1 and were used to calculate the amount of organic and inorganic material in each sample. However, the amount of Ca plus Mg, if assumed to be exclusively due to the minerals calcite, $CaCO_3$, and dolomite, $CaMg(CO_3)_2$, predicts carbonate contents higher than those from the acid CO_2 tests. To arrive at a value for CO_2 content, we eventually took the simple average of the two possiblities for each sample. The inorganic carbon was then calculated and subtracted from the total carbon to yield the organic carbon value.

Spent Shale Experiments and Results

Using the 30 to 100 mg pellets described above, several experiments were performed on each spent shale at 705°C. This temperature was chosen because organic combustion is rapid, while carbonate decomposition is slow (13), giving us an opportunity to partially separate the heat effects.

In one set of experiments, the calorimeter sample chamber was continuously swept with nitrogen at flow rates ranging from 115 to 210 cm^3/min, and samples were dropped from room temperature into 705°C. From the endothermic peak in the thermopile signal, a peak-height and a peak-area enthalpy value were calculated for the process

$$\text{spent shale (25°C)} \rightarrow \text{pyrolyzed shale + products (705°C)} \qquad 2)$$

Because of the slow carbonate decomposition, a long tail is evident on the peak, and there is a considerable difference between the peak-height and peak-area enthalpies (see below, Figure 2). In separate experiments, samples of spent shale were also dropped directly into the humidified oxygen stream (20 cm^2/min) to determine the total enthalpy

$$\text{spent shale (25°C)} + O_2\ \text{(705°C)} \rightarrow \text{burnt shale (705°C)} + CO_2,\ H_2O,\ \text{etc. (705°C)} \qquad 3)$$

A typical thermopile signal showed a number of events. It first moved in the endothermic direction to record sensible heat but then quickly changed to the exothermic direction to record rapid combustion. Finally, it returned endothermic to continue recording slow carbonate decomposition. The character of the signal depends on the balance between organic material and carbonate minerals in the sample. For peaks of this type, the peak-height value is meaningless, and the area from initial to final baselines was used to calculate the enthalpy.

Figure 2 shows all of the experimental results from the nitrogen experiments (height and area) and from the oxygen experiments (area only), plotted vs. the percent organic carbon on the spent shale samples.

Experimental Heat of Combustion and Comparison to Literature

When the peak-area value from the nitrogen drop (Equation 2) is subtracted from that of the oxygen drop (Equation 3) the result is the heat of combustion of spent shale at 705°C, including shale volatiles:

$$\text{(pyrolyzed shale + products)} + O_2 \rightarrow \text{burnt shale} + CO_2,\ H_2O,\ \text{etc.} \qquad 4)$$

We assume that all processes which occur under nitrogen also occur to the same extent under oxygen and that the combustion is then an additive contribution. In particular, both the carbonate decomposition enthalpy and any enthalpy of producing volatiles from the spent shale cancel in the subtraction. The enthalpy of volatiles production is expected to be small, and the carbonate decomposition enthalpy can be added back to give an adjusted form of Equation 4:

$$\text{spent shale (including carbonate)} + O_2 \rightarrow \text{burnt shale} + \text{mineral } CO_2 + CO_2,\ H_2O,\ \text{etc.} \qquad 5)$$

The experimental combustion values for Equation 5 are given in Table 2, where they are compared to literature values derived as follows.

Burnham et al. (14) report a correlation which represents the heats of combustion of spent Green River oil shales as determined by classical bomb combustion calorimetry. Since these heats refer to a set of specified standard states which are not typical of those expected at high temperatures, they adjust their correlation and give the following (their Equation 4) for the heat of combustion expected at high temperatures

$$\Delta H\ (J/g) = -375.3\ (\%\ \text{organic C}) - 512.5\ (\%S) + 20.85\ (\%\ CO_2) \qquad 6)$$

We have adjusted this further to change the final state for water from liquid to gas (by changing the term for % organic C from -375.3 to -368.0 as they recommend) and to change the final state for nitrogen from N_2 to a mixture of NO and NO_2. The resulting equation then assumes that the following processes occur: combustion of organic material, combustion of organic sulfur and inorganic sulfides, capture of SO_2 as sulfates, and decomposition of carbonates. However, one important question concerning the combustions at 705°C in our calorimeter is whether calcium and magnesium oxides have reacted with SiO_2 to form new silicate compounds. Literature indicates that the rates of these reactions are enhanced by steam (13), but we do not know whether the low level of moisture in our oxygen is enough to have a significant effect. Thus, in Table 2 we have calculated "literature" values in two ways, assuming either no silicate formation or complete silicate formation, using the terms given by Burnham et al. (14).

In Table 2, the overall agreement between our new data and the literature values, even toward the richer fractions, shows that to first order the heat of combustion at high temperatures is understood fairly well. However, as Burnham et al. (14) also concluded (concerning their bomb calorimetry

results), there are important questions remaining, particularly on the role of mineral reactions. For example, the experimental scatter does not permit a definitive statement on the occurrence of silicate reactions in our calorimeter, since some of the points in Table 2 support one assumption and some the other.

CONCLUSION

High-temperature Calvet calorimetry is a powerful means of determining accurate enthalpy values for oil shale processes at high temperatures, using very small samples (50 to 200 mg). By using samples from sink-float separation procedures (7), a wide range of organic and inorganic contributions can be studied. In a previous paper (3), values for the heat of retorting Green River oil shales to 500°C have been extended beyond the oil yields previously studied (5,15), and the first accurate values for Rundle shales were determined. To our knowledge, the present study also represents the first attempt to measure heats of combustion of spent shales in a high-temperature calorimeter (i.e. other than by differential scanning calorimetry or differential thermal analysis). Results for spent Green River oil shales at 705°C agree reasonably well with those derived from classical bomb calorimetry, but there are important questions remaining on the contributions of mineral reactions to the enthalpy.

ACKNOWLEDGEMENT

We thank Charles J. Vadovic for providing us with the valuable series of sink-float samples and the many colleagues at Exxon who have offered valuable comments and suggestions during the course of this work.

REFERENCES

1. Mraw, S. C.; Keweshan, C. F. J. Chem. Thermodynamics 1984, 16, 873.
2. Mraw, S. C.; Keweshan, C. F. Ind. Eng. Chem., Fundamentals 1985, in press. (See also, AIChE Spring National Meeting, May 20-23, 1984, Anaheim, California, USA.)
3. Mraw, S. C.; Keweshan, C. F., paper submitted to Fuel.
4. Mraw, S. C.; Kleppa, O. J. J. Chem. Thermodynamics 1984, 16, 865.
5. Wise, R. L.; Miller, R. C.; Sohns, H. W., U.S. Bureau of Mines, 1971, Report of Investigation 7482.
6. JANAF Thermochemical Tables. Stull, D. R.; Prophet, H., directors. 2nd ed. NSRDS-NBS 37: U.S. Government Printing Office, Washinton, DC 1971.
7. Vadovic, C. J. Prepr. Am. Chem. Soc. Div. Fuel. Chem. 1983, 28(3), 148.
8. Union Carbide Corporation, Carbon Products Division, New York, New York.
9. Stull, D. R.; Westrum; E. F., Jr.; Sinke, G. C., The Chemical Thermodynamics of Organic Compounds, Wiley: New York, 1969.
10. We thank James E. Hardy of this laboratory for this valuable suggestion.
11. Analabs, Inc., 80 Republic Dr., North Haven, Connecticut 06473.
12. Galbraith Laboratories, Inc., P. O. Box 4187, Knoxville, TN 37921.
13. Burnham, A. K.; Stubblefield, C. T.; Campbell, J. H. Fuel 1980, 59, 871.
14. Burnham, A. K.; Crawford, P. C.; Carley, J. F. Ind. Eng. Chem. Process Des. Dev. 1982, 21, 485.
15. Carley, J. F., Lawrence Livermore National Laboratory, private communication, to be published.

Table 1

Analyses of Green River Shale Samples Retorted by TGA to 500°C (Galbraith Laboratories (12))

Sample	C (total)	% of dried spent shale H	N	S	Ca	Mg	ash	carbonate C	SO_3 (% on ash)
2.2S	8.74	0.27	0.29	0.81	16.60	3.96	74.75	6.64	2.80
2.2F	9.48	0.28	0.33	0.70	17.74	4.03	74.27	6.53	2.89
2.0F	9.54	0.32	0.42	0.98	14.97	4.06	75.73	5.76	3.20
1.9F	10.24	0.45	0.65	1.36	10.89	3.96	78.03	4.52	4.89
1.8F	11.19	0.56	0.71	1.60	9.63	3.71	77.36	4.13	5.74
1.7F	12.16	0.59	0.80	2.06	8.60	3.36	78.13	3.76	7.04
1.6F	12.10	0.61	0.79	2.34	8.62	2.66	78.82	3.19	6.57

Table 2

Experimental values, derived from the present work, for the heat of combustion of spent Green River oil shale at 705°C, and comparison to values derived from bomb calorimetry (14); see text.

sample	organic C (% spent shale)	$-\Delta H_c$ (kJ/g of spent shale) this work[a]	Reference 14 w/o silicates	Reference 14 w silicates
2.2S	1.96	0.34 ± 0.05	0.22	0.59
2.2F	2.56	0.79 ± 0.14	0.36	0.75
2.0F	3.42	1.15 ± 0.06	0.93	1.26
1.9F	5.37	2.26 ± 0.06	2.01	2.26
1.8F	6.77	2.57 ± 0.11	2.71	2.92
1.7F	8.16	3.37 ± 0.07	3.51	3.69
1.6F	8.56	3.77 ± 0.06	3.86	4.00

[a]Values given for each sample represent the average peak-area enthalpy from the oxygen drops minus that from the nitrogen drops and then adjusted to include carbonate decomposition, according to Equation 5 in the text.

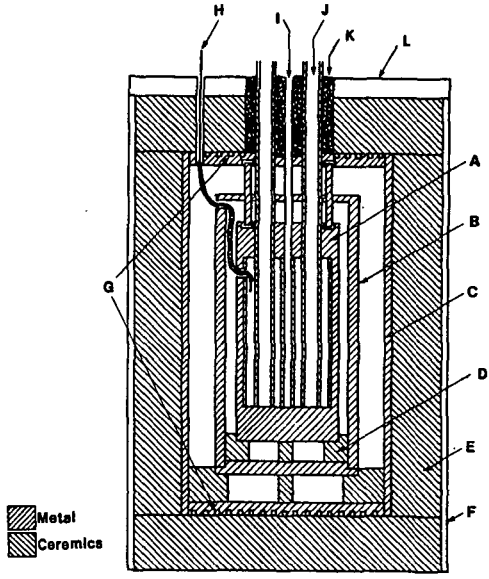

Figure 1

Assembly diagram of the high-temperature calorimeter (overall dimensions: h=80 cm; d = 65 cm). A: Inconel block; B: temperature homogenizing shield; C: furnace shell; D: ceramic support blocks; E: cast refractory insulation; F: side water jacket; G: grooves for top and bottom heater wires; H: typical thermopile lead wire; I: central well for precision thermocouple; J: ceramic tube sample chamber; K: ceramic wool; L: top water jacket.

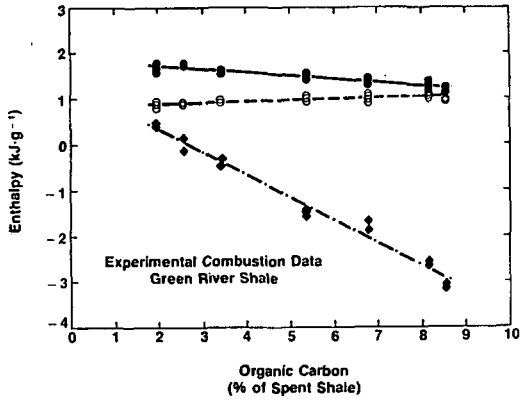

Figure 2

Experimental enthalpy values determined from drops of spent Green River shale into nitrogen or oxygen at 705°C, vs. the percent organic carbon on spent shale.

o, — — — nitrogen peak height
●, ——— nitrogen peak area
◆, — • — oxygen peak area

A NEW MODEL OF KEROGEN STRUCTURE

By

C.J.R. FOOKES and D.A. JOHNSON

CSIRO Division of Energy Chemistry, Lucas Heights Research Laboratories,
Private Mail Bag 7, Sutherland, NSW 2232, Australia.

INTRODUCTION

By far the most prominent components of a typical shale oil are n-alkanes and n-alkenes, which form a homologous series extending to C_{30} or beyond. Since it is now clear that these molecules are readily converted into aromatics and branched aliphatics under retorting conditions(1), it is likely that n-alkanes and n-alkenes are the major primary products of kerogen pyrolysis. Knowledge of how they are generated is thus of crucial importance to oil shale chemistry, particularly with respect to the nature of kerogen.

Although the literature abounds with proposals for the structure of kerogen, most are based on the results of oxidative degradations(2). Although these experiments provide useful information about individual structural fragments, very little can be learned about the way in which they are linked, since virtually all functional groups are converted into carboxylic acids. Nevertheless, it is generally accepted that kerogen is composed of both aliphatic and aromatic structures, with the most convincing evidence for the latter coming from solid-state ^{13}C nuclear magnetic resonance (NMR) and infrared studies of intact kerogens and shales.

We have made the assumption that the aromatic and aliphatic moieties are associated, and that kerogen consists mainly of n-alkyl chains attached to a largely involatile aromatic (or more likely heteroaromatic) nucleus. On pyrolysis, the aliphatic side chains are cleaved to form oil, whereas most of the hydrogen-deficient nucleus forms coke. To test this hypothesis, we have pyrolysed a range of appropriate model compounds, 1 - 5, and compared the products and kinetics of their decomposition with data obtained from oil shales.

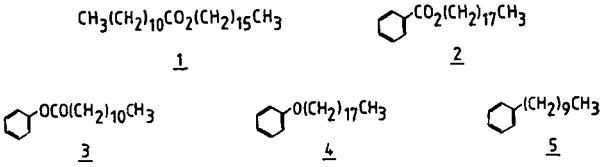

EXPERIMENTAL

Pyrolyses were carried out in a quartz flow tube enclosed in the oven of a gas chromatograph. The compounds were transferred in a stream of helium from an evaporation chamber held at a temperature (usually around 200°C) sufficient to give a partial pressure of reactant of approximately 150 Pa. The products were collected in U-tubes immersed in liquid nitrogen and analysed by ^{1}H NMR using a JEOL GX400 spectrometer. For each compound, the residence time was constant but the reactor temperature was varied to give between 5 and 50% decomposition.

Activation energies were then calculated from a plot of log x v. 1/T, where x is the fraction decomposed at temperature T (in K). Rate constants (k) were calculated from the formula $kt = \ell n(1-x)$. Solid state ^{13}C spectroscopy was performed on a Bruker CXP300 instrument, using the Dixon total side-band suppression sequence(3).

RESULTS AND DISCUSSION

Support for the presence of n-alkyl chains is gained from the high field solid-state ^{13}C NMR spectrum of a Condor carbonaceous kerogen (Figure 1, upper trace). The lower trace is the solution spectrum of a carbonaceous shale oil for comparison. Particularly noteworthy is the correspondence of signals A and D between the two spectra, which shows that long n-alkyl chains, free at one (or each) end, are present in the kerogen.

Information about the site of attachment of these chains was provided by ^{13}C NMR examination of the alkene fraction isolated from a Condor oil. Although the occurrence of 1-enes in shale oils is well documented, there is very little information on the distribution of other double-bond isomers. Figure 2 shows that high field ^{13}C NMR is an excellent method for determining this distribution, at least for the first five or six carbons along the chain, giving cis/trans ratios as well.

The quantitative data from this spectrum were best interpreted as indicating that 1-enes are in fact the initially-formed olefins and that the double bond then migrates along the chain.* Thus the terminal carbon is the likely site of their original linkage to the kerogen. This is consistent with the widespread occurrence in the biosphere of long-chain fatty acids and, to a lesser extent, primary alcohols and their isolation from the hydrolysis of kerogens(4). We have therefore based the following models on these two classes of compounds and used the benzene ring as the simplest aromatic nucleus.

Hexadecyl dodecanoate - 1. This wax ester pyrolysed readily between 430 and 460°C to give almost exclusively 1-hexadecene and dodecanoic acid. Significantly, very little n-undecane was formed. The reaction was shown to be first order by varying the partial pressure of substrate between 40 and 600 Pa; except at the lowest concentration, no significant change in the fractional decomposition at 450°C was observed. The calculated activation energy and rate constant at 450°C are given in Table 1, together with the corresponding parameters for the evolution of hydrocarbons by pyrolysis of several oil shales. As can be seen, neither the kinetics nor the products of this reaction correspond well with those from oil shales.

Octadecyl benzoate - 2. This ester decomposed even more readily than the previous compound, giving 1-octadecene and benzoic acid as almost the only products. However, a small amount of benzene was also formed, presumably from decarboxylation of the benzoic acid. Thus, this compound cannot be considered a good kerogen model.

Phenyl dodecanoate - 3. Phenolic esters of fatty acids have been implicated in the structure of humic substances(9) such as those derived from lignins. It was therefore interesting to discover that although phenyl dodecanoate pyrolysed rather slowly, the activation energy for its decomposition is similar to that

---

* dehydrogenation of alkanes is an additional pathway(1), leading to a significant proportion of olefins with a random distribution of double-bond positions.

for Nagoorin carbonaceous shale, which contains large quantities of lignitic materials. Furthermore, the major products derived from the side chain were n-undecane and 1-decene (Figure 3). Pyrolysis of phenolic esters of a natural series of carboxylic acids, where even numbered chains predominate, should therefore generate n-alkanes with odd over even preference and 1-enes with a less pronounced even over odd preference. This is often observed in shale oils.

Phenyl octadecyl ether - 4. The decomposition kinetics of this compound were complicated. Above about 460°C, the reaction appeared to have an activation energy of less than 200 kJ mol^{-1}, whereas at lower temperatures the value was more than 500 kJ mol^{-1}. This probably indicates that the initial bond-cleavage is not the rate-determining step below 460°C, but it may be above this temperature. The products were even more complex; their chromatogram is shown in Figure 4.

Note the homologous series of n-alkanes dominated by heptadecane, and the more abundant series of 1-enes, with 1-octadecene the major compound. Phenol and, unexpectedly, benzaldehyde are the major aromatic products, although styrene and various alkylbenzenes including n-heptadecylbenzene were also identified. In addition, products arising from the random scission of the side chain of 4 are present in significant amounts.

Although the products and rate of decomposition of this compound correspond well to those of oil shales, the complicated activation energy precludes a decision about its validity as a kerogen model.

Decylbenzene - 5. This compound, which represents the simplest linkage of an alkyl chain to an aromatic ring, pyrolysed extremely slowly, although its activation energy was virtually identical to those reported for the decomposition of typical oil shales. The major products were styrene, toluene, ethylbenzene and 1-nonene; only very small amounts of n-alkanes were detected. As with the previous compound, there was also cleavage of carbon-carbon bonds along the side chain.

CONCLUSIONS

Of the five compounds pyrolysed in this study, only phenyl dodecanoate can be considered as a good model of kerogen structure, but only for the carbonaceous shales. None of the other compounds, with the possible exception of phenyl octadecyl ether, adequately mimicked either the high or low activation energy processes of oil shale pyrolyses.

The nature of the higher activation energy process is rather intriguing. The fact that roughly equal quantities of n-alkanes and alkenes are generated by the rapid pyrolysis of shales and kerogens suggests that the two classes of compounds have a common origin; indeed kinetic data(7,8) indicate that a single rate-determining process is involved in the formation of the bulk of the oil. We believe that this process involves the generation of primary n-alkyl radicals which would then disproportionate to give equal quantities of n-alkanes and 1-alkenes. Certainly, other have provided evidence for the involvement of radicals in kerogen pyrolysis(10). However, the reaction which produces these radicals has yet to be elucidated.

ACKNOWLEDGEMENTS

We thank Ms C. Walters and J. Wymer for syntheses of model compounds and NMR measurements, Mr. I. Liepa and Dr. A. Chaffee for GC/MS data, Mr. J. Levy

for the use of a least-squares analysis program, and Dr. J.K. Saunders (University of New South Wales) for assistance in determining the solid-state NMR spectrum. We are also grateful to Dr. A. Ekstrom for helpful discussions and permission to quote unpublished data.

LITERATURE CITED

1. Regtop, R., Ellis, J., Crisp, P.T., Ekstrom, A. and Fookes, C.J.R., Proceedings of the Second Australian Workshop on Oil Shale, Brisbane, December 1984, p. 170.

2. For a review, see D. Vitoric in 'Kerogen', Ed. B. Durand, Editions Technip, Paris, 1980, p. 301.

3. Dixon, W.T., Schaefer, J., Sefcik, M.D., Stejskal, E.O. and McKay, R.A., J. Magn. Resonance, 49, 341 (1982).

4. Regtop, R.A., PhD. Thesis, University of Wollongong, NSW, Australia (1983).

5. Campbell, J.H., Koskinas, G.J. and Stout, N.P., UCRL-50289 (1976).

6. Calculated, assuming first-order kinetics, from the data of Charlesworth, J.M., Proceedings of the First Australian Workshop on Oil Shale, Lucas Heights, May 1983, p. 127.

7. Ekstrom, A., Hurst, H.J. and Randall, C.H. ibid., p. 123.

8. Ekstrom, A., unpublished results.

9. Schnitzer, M. and Negroud, J.A. Fuel, 54, 17, 1975.

10. Solly, R.K., Charlesworth, J.M., Beranek, L.A., Kelso, A.G. Moritz, A.G. and Power, A.J., Proceedings of the First Australian Workshop on Oil Shale, Lucas Heights, May 1983, p. 113.

TABLE 1
ACTIVATION ENERGIES AND RATE CONSTANTS AT 450°C FOR THE DECOMPOSITION OF MODEL COMPOUNDS AND GENERATION OF OIL FROM SHALES

Substance	Activation Energy kJ mol^{-1} ($\pm$ 1 σ)	Rate Constant (450°C) s^{-1}
Hexadecyl dodecanoate	172 ± 2	1.78×10^{-2}
Octadecyl benzoate	163 ± 2	2.21×10^{-2}
Phenyl dodecanoate	147 ± 7	1.60×10^{-3}
Phenyl octadecyl ether	see text	4.26×10^{-3}
Decylbenzene	222 ± 5	4.45×10^{-5}
Green River shale (5)	219	3.95×10^{-3}
Rundle shale		5.8×10^{-3} (6)
Rundle kerogen		7.7×10^{-3} (6)
Condor shale (7)	232	1.73×10^{-3}
Nagoorin carbonaceous shale (8)	152	5.22×10^{-3}

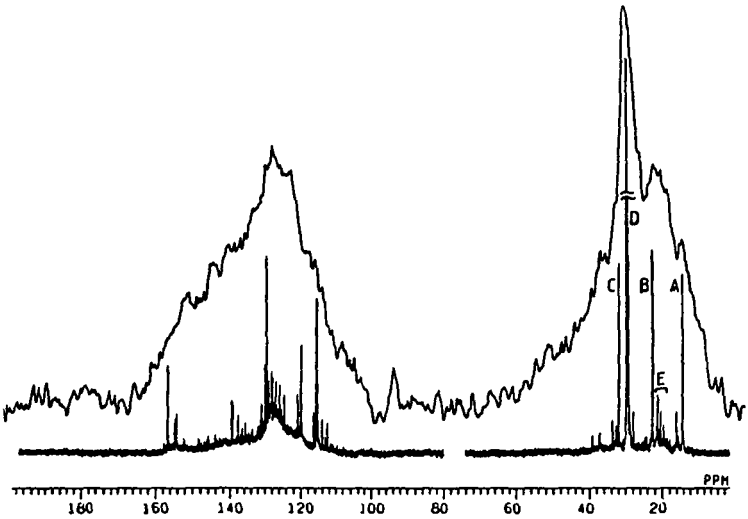

FIGURE 1: (Upper trace) 75 MHz CPMAS ^{13}C NMR spectrum of a Condor carbonaceous kerogen. (Lower trace) solution ^{13}C spectrum of a carbonaceous shale oil showing signals due to A, terminal methyls (C-1); B, C-2; C, C-3; and D, C-4+ of n-alkyl chains, and E, aromatic methyls. Most of the sharp lines in the aromatic region (110-160 ppm) are from phenols.

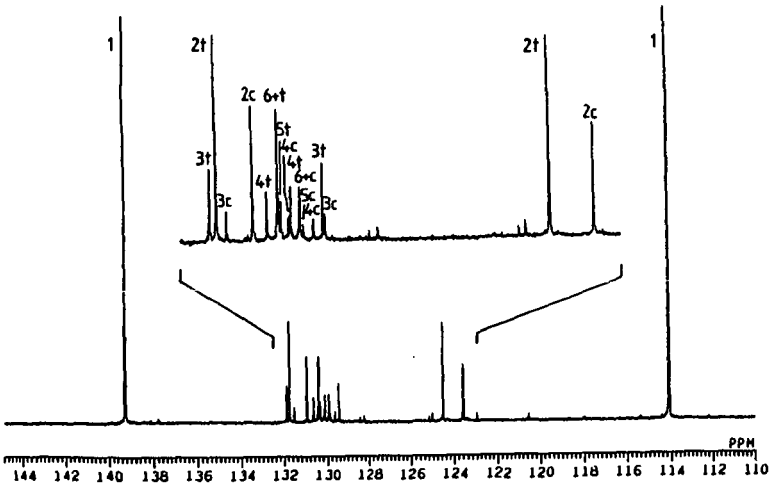

FIGURE 2: Olefinic region of 100 MHz ^{13}C NMR spectrum of the alkene fraction from Condor shale oil. The label 2t (for example) refers to signals from straight chain trans-2-enes.

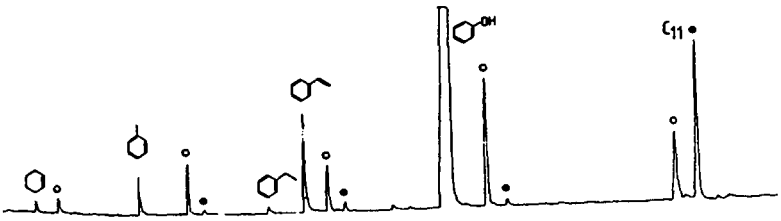

FIGURE 3: Reconstructed ion chromatogram of products from the decomposition of phenyl dodecanoate: ● = n-alkanes, o = 1-alkenes.

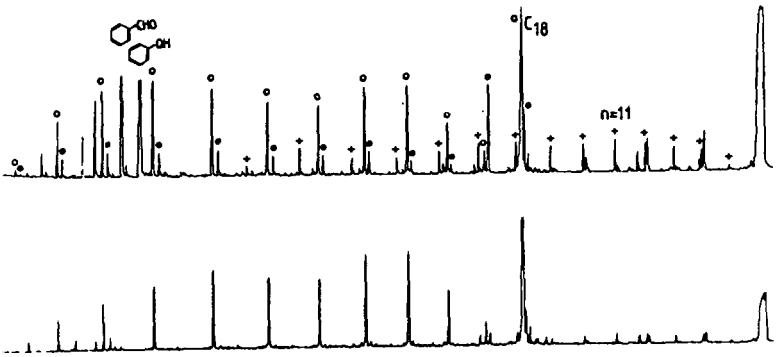

FIGURE 4: Reconstructed ion chromatogram of products from the decomposition of phenyl octadecyl ether; + = $C_6H_5O(CH_2)_nCH{=}CH_2$.

INORGANIC NITROGEN IN GREEN RIVER FORMATION OIL SHALE*

R. W. Taylor
A. K. Burnham
G. S. Smith
R. H. Sanborn
L. S. Gregory

Lawrence Livermore National Laboratory
Livermore, California, 94550

ABSTRACT

Inorganic (mineral) N has been found in both raw and retorted Green River Formation oil shale. Buddingtonite, an ammonium-bearing feldspar, has been identified in some shales by X-ray diffraction, and ammonium ion (NH_4^+) has been found in the same and other shales by infrared adsorption. Measurement of total N content of low-temperature ashed oil shale by a combustion technique is proposed as a method of measuring inorganic-N content. The method is based on the observation that the N content of buddingtonite is not reduced by low temperature ashing. Use of this technique demonstrates that inorganic N content is variable and is the major source of nitrogen in some oil shale samples. The fate of both organic and inorganic N during pyrolysis is also discussed.

INTRODUCTION

Within the United States are large and rich deposits of oil shale. Formost of these is the oil shale of the Green River Formation of Colorado and Utah. This shale contains approximately 0.5 wt% N, but the concentration is variable, ranging from 0.2% to as much as 1%. Pyrolysis of oil shale produces ammonia which needs to be removed from the retort water before recycling or disposal (1). N in shale oil must be reduced to produce stable, non-polluting transportation fuels, and removal of N requires special catalysts and consumes H increasing the cost of refining (2). Nitric oxide (NO) is produced when retorted shale is burned as a fuel (3,4).

The ratio of N to organic C both in samples of Green River oil shale and in kerogen isolated from the same samples has been measured but only a slightly higher ratio in whole shale than in kerogen, was found suggesting that most of the N (90%) is organic (5,6). This is qualitatively consistent with the observation by most workers that N content of oil shale increases with an increase in grade or organic C content (6-9). However, correlation of organic C with N does not prove that N is organic; N may have originated in organic debris, but has been transferred to the inorganic matrix during diagenesis. Finally, some of the published data on N content as a function or organic C content show a non-zero intercept (7-9), suggesting shale contains some N even in the absence of organic C.

Recently, Cooper and Evans (10) utilized HF-HCl digestion in the determination of inorganic N and concluded, in conflict with prevailing opinions, that most N in both raw and retorted shale was inorganic in form. Later, Nadkarni (11) showed that the measured "total" N content for some shales depended on the technique used. For a sample of Colorado shale, the Kjeldahl method measured a N concentration of 0.45±0.05% while combustion (Dumas) methods gave a value of 0.74±0.16%. These two papers cast doubt about the data on which the previous conclusions have been based.

Most of the N in the Condor oil shale deposit of Australia is inorganic. It is found as an ammonium silicate of the feldspar family called buddingtonite, and the concentration of this mineral in the Condor shale is approximately 10 wt% (12).

The purpose of this report is to put proper perspective on the occurrence and abundance of inorganic N in Green River oil shale.

EXPERIMENTAL SECTION

All samples used in this investigation were ground to a talc-like consistency in a rotating concentric disk and ring (Bleuler) mill before analysis. Past experience indicates that essentially all material prepared by this procedure passes a 325 mesh sieve and most was >10μ in diameter. Some samples were treated with 1 M HCl overnight to remove carbonate minerals.

Some samples were low-temperature ashed in an oxygen plasma (LEF Corp. LTA-504) to remove organic matter. The oxygen pressure was maintained a 1 torr, and the total power in each of the four chambers was 250 watts.

Carbon, H and N content were measured at LLNL by either a Perkin-Elmer Model 240 or Leco model CHN-600 elemental analyzer. The samples size for the Perkin-Elmer instrument was 2-4 mg, and the sample size for the Leco instrument was 100 mg. To ensure good precision 3 to 4 replicates were measured for each reported value. Organic C was determined by the difference between total C and that evolved by 1 M HCl and collected on ascarite. Although the reproducibility among determinations of N concentration of a given sample at a given time was generally ±0.02 wt% N, the agreement among groups of N analyses for the same shale over a period of several years was not as good. The reasons for this are not clear. Because of this problem some samples were sent to J&A Associates, Golden, Colorado, for measurement of total N by means of an Antek Chemiluminescence Analyzer Model 707.

A Digilab Model FTS-20c infrared spectrometer was used to measure the infrared spectrum in the transmission mode. Each sample was diluted to approximately 2% in KBr and pressed into a pellet.

A Phillips Diffractometer was used to determine the x-ray powder patterns. Early patterns were recorded on strip-chart recorders, but recent patterns were recorded and processed by computer.

A sample of buddingtonite, identified as California 117751-6, was acquired from the Smithsonian Institution (13). The N content was measured at 1.69% at LLNL and 2.78% at J&A Associates.

A description of the oil shale samples used is given in Table 1. Most of them have been used in other investigations at LLNL or other laboratories. The chemical analyses are values averaged from at least 3 samples from the same batch of shale determined at different times.

RESULTS

Identification of buddingtonite in oil shale by x-ray diffraction

Buddingtonite was first discovered in oil shale (sample L-1 9A/5) by G. Smith at LLNL in 1976 as part of a routine x-ray analysis of raw shale to be used in the L-1 retorting experiment (15). Buddingtonite was also identified in raw and retorted shale (sample RI 8008-76) in an unpublished 1978 investigation on the analysis of dawsonite in oil shale.

Table 2 compares d-spacings for 10 strongest x-ray diffraction peaks of buddingtonite, based on the ASTM standard #17-517, to those from our measurements of the Smithsonian Institution (SI) sample of buddingtonite. Peaks apparently due to buddingtonite in two Colorado oil shale samples and one sample of buddingtonite

Table 1
Green River Oil Shale Samples

#	I.D.	Location	Oil Yield (gpt)	Chemical Composition, Wt%						%Inorg. N[a]
				C	acid CO_2	org. C	H	S	N	
1	Ca37	Tract Ca	34.3	21.90	15.98	17.5	2.38	--	0.61	21
2	Ca25	Tract Ca	24.8	16.57	19.67	11.2	1.68	1.1	0.54	43
3	AP60	Anvil Points	61.0	30.38	12.32	27.0	3.55	0.84	0.95	22
4	AP31	Anvil Points	30.6	19.63	20.55	14.0	1.84	--	0.43	10
5	AP24	Anvil Points	22.4	15.60	17.48	10.8	1.62	0.63	0.41	27
6	AP8	Anvil Points	8.1	9.95	21.44	4.1	0.57	0.23	0.12	13
7	RI8008-76	Co.Core #3[b]	22.0	12.56	12.32	9.2	1.71	1.35	1.16	78
8	USNOSR-638	Naval Reserve-1	1.9	4.65	11.40	1.5	0.46	0.87	0.54	92
9	L-1(9A/5)	Anvil Points	25.0	15.64	17.12	11.0	1.56	0.69	0.47	35
10	GK5	Geokinetics,Ut.	4.7	6.53	15.20	2.4	0.51	--	0.20	67
11	HD25	Horse Draw, Co.[c]	25.0	19.20	29.50	11.1	2.02	0.60	0.45	32

a) Fraction of inorg. N = $\frac{\%N-0.0276(Org.C)}{\%N}$ (see discussion)

b) Northern Piceance Creek Basin at ∿ 230m, dawsonite rich.

c) Multi Mineral Corp., 649m, nahcolite rich.

Table 2
Identification of the 10 strongest diffraction lines of buddingtonite in standards and oil shale samples.

I/Io	hkl	d(Å)				
		ASTM 17-517	SI	RI8008 No76	USNOSR 638'	CONDOR[a]
100	130	3.81	3.82	3.71	3.79	3.82
95	010	6.52	6.52	6.52	6.52	6.52
70	220	3.38	3.35[b]	3.35[b]	3.34[b]	3.386
70	202	3.25	3.24	3.24	3.23	3.2226
65	101	4.33	4.50[b]	4.50[b]	4.48[b]	4.33
60	040	3.26	3.24	3.24	3.29	3.260
40	140	3.01	3.02	3.02	3.00	3.013
35	011	5.91	5.92	5.92	5.90	5.92
35	211	3.98	3.98	3.95	3.96	3.98
35	002	3.31	3.35[b]	3.35[b]	3.34[b]	3.320

[a] Ref. (12).

[b] Spacings probably influenced by contributions from strong quartz peaks at d=3.47 and 4.25Å.

separated from Australian (Condor) shale are also compared in Table 2. The SI sample contains a large percentage of quartz, and the Green River Oil Shale samples contain large fraction of quartz, dolomite, and some dawsonite.

Our first evidence that buddingtonite is thermally stable came from its identification sample RI 8008-76 that had been heated to about 500°C in a covered crucible for one hour. Little of the carbon residue had been oxidized, so that this treatment roughly approximated Fischer Assay heating. Figure 1 compares the diffraction patterns of the raw and heated oil shale. The buddingtonite peaks are the same. In contrast, the dawsonite peaks are missing, confirming that the sample was heated above 350°C. We have also found that buddingtonite releases nitric oxide (NO) during oxidation after being heated to 500°C in an inert gas (4). The amount of NO was not effected by duration of preheating within the range 3 to 10 min. which indicates that the rate of ammonium release at 500°C is slow. These observations are consistent with (12) who found the x-ray diffraction patterns of buddingtonite does not change below 500°C. They found, in addition, that ammonium is lost by heating to 650°C, that remnants of the feldspar structure remains even upon heating to 750°C and that buddingtonite was not reformed by heating in a NH_4OH solution at 180°C.

Ammonium ion identification in oil shale by infrared spectroscopy

Buddingtonite has a characteristic band at 1430 cm^{-1} which distinguishes it from other silicates. The IR spectrum of our SI reference sample of Buddingtonite (13) is shown in Figure 2. The large adsorption in the 900-1300 cm^{-1} region is characteristic of the Si-O stretch. Bands in the 600-800 cm^{-1} region can be due to hydrocarbons as well as silicates. The ammonium ion has another adsorption band in the 3000-3500 cm^{-1} region, but it is strongly overlapped by water bands, making it less characteristic.

In Green River oil shale, the 1430 cm^{-1} band is overlapped by CH bending modes and also from a bending mode in the carbonate ion. Thus, to identify the ammonium ion definitively, it is necessary to remove organic material and carbonate minerals. Figure 3 shows an IR spectrum of sample AP24 that has had carbonate minerals removed by acid leaching. One would not ordinarily suspect the presence of ammonium ion because of the CH bending mode at 1350 to 1410 cm^{-1}. However, when organic material is removed by low-temperature ashing (using procedures described in detail in the next section), the ammonium-ion band emerges clearly, although not to the same relative intensity as in the spectrum of the SI buddingtonite or in the spectrum of buddingtonite reported by Loughnan and Roberts (12).

Figure 4 shows IR spectra of samples AP8 and AP60 after HCl leaching and low-temperature ashing. Sample AP8 shows little adsorption and sample AP60 shows none, which agrees with data on nitrogen content discussed in the next section.

Isolation of inorganic N by low-temperature ashing

The occurrence of inorganic N in Green River oil shale is clear based on x-ray and infrared evidence presented thus far, but a quantitative method of analysis for inorganic N is needed. While both x-ray diffraction and infrared spectroscopy have been used for quantitative mineral analysis, all of the inorganic forms of N have not necessarily been identified. In this section, a low-temperature ashing technique is developed for determination of inorganic N.

The most important variables in low-temperature ashing of oil shale are time, particle size, sample-stirring frequency and plasma activity. We have found that using 1 torr of O_2 and a power of 250 watts removed oil shale organic matter.

The role of particle size on the effectiveness of low-temperature ashing is shown in Figure 5. Both samples came to constant weight within 35 hours of ashing. The weight loss of the finer sample was 13.2%, which is about equal to the weight loss upon Fischer assay (12.84%) but the coarser sample lost only 9.3%. The time necessary to come to constant weight was cut in half if carbonates were removed with HCl before ashing.

The relative loss of organic C, H, and N during low-temperature ashing of Anvil Points shale, sample L-1 (9A/5), is shown in Figure 6. It is unlikely that organic C could be oxidized without also oxidizing organic H and N, so residual content of H and N is probably due to mineral forms.

Since buddingtonite is the only specific N-bearing mineral that has been identified in oil shale, we used it to test whether or not low-temperature ashing affects mineral N content. Table 3 gives total N content for a fine-ground sample of SI buddingtonite before and after being ashed for 35 hours (sample #12). The measured value of N content depended on the type of analysis being used, but the fraction of N remaining was over 90% by either analytical technique. This agrees with the qualitative observation in the previous section that ammonium-ion, as detected in the infrared spectrum, is not affected by ashing.

Table 3 also lists N content for a variety of raw and retorted oil shales before and after low-temperature ashing. The retorted samples were prepared by a modified Fischer Assay technique (16). The fraction of N removed by ashing ranges from nearly none to all. As discussed in more detail in the next section, this implies that the relative organic and inorganic N contents of Colorado oil shale are highly variable. Acid leaching of raw or retorted shale does not seem to make a systematic change in the fraction of N remaining after ashing, and the variation is probably a reflection of uncertainty in N concentration measurements.

DISCUSSION

One would think that a determination of the relative amounts of organic and inorganic N could be made by comparing N in whole shale to that in organic concentrates. Three workers have reported composition of raw shale and also the composition of the organic concentrates from the same shales from which the fractional recovery of N can be calculated (5-7). This is summarized in Table 4 along with a shale sample analyzed at LLNL. Approximately all of the N in raw shale is recovered in organic concentrate. This evidence has caused most workers to assume that the inorganic N content of oil shale is minor. In addition, elemental analysis of the organic material isolated from sample AP60 by Kirkman Bey and Campbell at LLNL indicated that all of the nitrogen in that sample is organic.

However, the results of (11) suggest that is not safe to use these results to conclude that there is little inorganic N in Green River oil shale. Using replicate results from several independent laboratories, (11) found that the Kjeldahl technique (digestion of the sample in hot concentrated sulfuric acid) gives systematically lower N values for Colorado oil shale than the Dumas (combustion) method. This is consistent with the need for HF digestion for the determination of fixed or "nonexchangeable" ammonium in soil and rock samples (17). If only organic N is detected by normal Kjeldahl analysis, it would be logical for most of it to be recovered in the organic concentrates even if greater quantities of inorganic N were present. Moreover, the rich oil shale used at LLNL is uniquely low in organic N.

A second way to estimate the relative abundance of inorganic N in either raw or retorted shale is to plot total N content verses organic C content. If the concentration of inorganic N is independent of organic C content and organic

Table 3
Wt%N in Raw, Retorted, and Low Temperature
Ashed Samples On a Raw Shale Basis

Sample #	Material	Wt% N			% of Raw Shale N Remaining After LTA (±10%)
		Raw	Retorted	LTA[a]	
1	Ca37	0.72	--	0.17	24
1	Ca37	0.72	0.35	0.15	21
2	Ca25	0.58	--	0.25[b]	43[c]
2	Ca25	0.47	--	0.31	66
2	Ca25	0.58	0.43	0.33[b]	57[c]
2	Ca25	0.47	0.49	0.20[b]	42
3	AP60	0.87	--	0.01[b]	1[c]
3	AP60	0.98	--	0.09[b]	9
3	AP60	0.87	0.28	0.02[b]	2[b]
3	AP60	0.98	0.45	0.06[b]	6
4	AP31	0.47	--	0.11	23
4	AP31	0.47	0.27	0.11	23
5	AP24	0.39	--	0.14	36
6	AP8	0.09	--	0.02	22
7	RI8008-76	1.13	--	0.72[b]	64
8	USNOSR-638	0.55	--	0.56[b]	102[c]
8	USNOSR-638	0.49	--	0.43[b]	88
9	L-19A/5	0.47	--	0.28[b]	59
10	GK5	0.32	--	0.28	56
10	GK5	0.32	0.22	0.19[b]	59
11	HD25	0.52	--	0.21	56
11	HD25	0.52	0.26	0.25	48
12	Buddingtonite	1.69	--	1.80[b]	107
12	Buddingtonite	2.78	--	2.58[b]	93[c]

(a) LTA of retorted shale if preceeded in table by retorted shale data, otherwise the LTA was done on raw shale.
(b) Acid leached (HCℓ) to accelerate ashing
(c) Chemical Analysis by J and A Associates, Inc. Golden, CO

Table 4
Comparison of N/org.C mole ratios for raw shale and organic concentrates from the same shales

N/Org.C Mole Ratio		Recovered	Reference
Raw Shale	Org. Concentrate	%N	
0.029 (a)	0.032	110%	(7)
0.027 (b)	0.025	93%	(6)
0.033 (c)	0.029	88%	(5)
0.029 (d)	0.016	89%	(5)
0.032 (e)	0.033	103%	LLNL

(a) Average of 9 samples, mineable beds, mahogany ledge (Anvil Points).
(b) Ten samples from the mahogany zone, 25 gpt.
(c) One sample, mahogany zone.
(d) One sample "papery" shale.
(e) One sample AP60, work done at LLNL.

Table 5
Nitrogen-organic carbon correlation

Data fit to expression: Wt%N=a+b(Wt% org. carbon)
Wt% N=total nitrogen content of sample
a=Wt% inorg. nitrogen
b=Wt ratio org. nitrogen/org. carbon

a	b	Samples	Sample Type and Location	Reference
			Raw Shale	
0.225	0.0275	260	2 core holes, USNOSR	(8)
0.096	0.0286	66	Colorado and Utah	(9)
-0.020	0.0320	40	1 core Utah, Geokinetics	LLNL Analyses
0.10	0.0249	6	1 sample split, Colony (Ca)	(18)
0.036	0.0307	9	Mineable beds, Anvil Points	(17)
0.252	0.015	6	Selected samples, Anvil Points	(7)
0.046	0.0318	58	Core KEP No 5, Kentucky	(18)
0.012	0.031	34	T16 Core, Kentucky	(19)
			Retorted Shale	
0.042	0.0665	66	Colorado and Utah	(9)
-0.009	0.069	9	"mineable" beds, AP	(7)
0.045	0.035	18	from NTU Retort[a]	(20)

[a] Some samples only partly retorted, some samples oxidized.

material has a constant N/C ratio, the slope of the plot gives the ratio of organic N to organic C, and the intercept gives the concentration of inorganic N. The observation that N content of oil is independent of grade (9) supports our assumption of constant kerogen composition. The results of linear regression analysis of several sets of data in the literature are given in Table 5, including data from two Kentucky oil shale cores, and some data for retorted shales.

A positive intercept is found for each set of samples except for those from the Geokinetics core from Utah which has a negative intercept of -0.020. The organic N to organic C wt ratio for Green River oil shales is 0.0276 which is a value calculated from the slopes in Table 4 weighted in proportion to the number of samples. The value of this ratio for retorted shale is 0.064.

A comparison of the fraction of inorganic N determined by the two methods for 11 shale samples is given in Fig. 7. Although a trend is clear considerable differences stand out for some samples.

The correlation coefficient for the linear regression analysis of N/org. C for the data of Giauque et al. (8) is 0.79. We feel that the observed random variation in N content (above a minimum value) for a given organic C content is due mostly to a variation in the inorganic N content.

With respect to the fates of organic and inorganic N during pyrolysis, we have shown that buddingtonite is relatively stable in the absence of air at temperatures up to 500°C and that inorganic N is not generally lost during retorting of shales, but the uncertainty is large due in part to the lack of accuracy in measuring N content in samples with low N concentrations.

CONCLUSIONS

On the average, approximately half of the N in the Green River Formation is inorganic, but the distribution is not uniform. Inorganic N in raw shale tends to remain in the shale after retorting. Buddingtonite, an ammonium feldspar, has been identified by means of x-ray diffraction in some oil shale samples. Ammonium ions have been identified in the same and other samples by means of infrared adsorption. Low-temperature ashing of oil shale by means of an oxygen plasma has been found to remove organic N, but not inorganic N in buddingtonite. Measurement of total N after low-temperature ashing is proposed as a way of determining inorganic N content. Due in part to the difficulty of measuring N concentration is samples with little N the method is qualitative. A second method for the estimation of the inorganic N content of shale is based on the assumption that the org. N/org.C ratio is constant. At present it is not clear if one estimate is better that the other.

In view of the present results, the stoichiometry of retorting must be revised. Organic material in raw shale and in the char in retorted shale contains less N than previously thought. The CH&N composition of organic material in raw shale should be represented by the formula $CH_{1.50}N_{0.024}$. The chemical composition of organic material in retorted shale should be represented by the formula $CH_{0.42}N_{0.06}$.

Acknowledgment

We thank J. S. White, Associate Curator-in-Charge, Division of Mineralogy, U.S. National Museum of Natural History, Smithsonian Institute, for providing us with a reference sample of buddingtonite. We also acknowledge the C-N correlations by D. Fujimoto and T. Coburn of LLNL.

References

(1) Gibbons, J. H., Director,"An Assessment of Oil Shale Technologies," Office of Technology Assessment, U.S. Congress, U.S. Government Printing Office, Washington, D.C. 20402, Stock No.052-003-00759-2, 1980.

(2) Wasilk, N. J. and E. T. Robinson, in Oil Shale, pp. 224-235 in Tar Sands, and Related Materials, H. C. Stauffer Ed., ACS Symposium Series 163, 1981.

(3) Lyon, R. K. and J. E. Hardy, Combustion and Flame, V. 51, pp. 105-107, 1983.

(4) Taylor, R. W., C. J. Morris and A. K. Burnham, Lawrence Livermore National Laboratory, Report UCRL-90155,1985, to be presented at the 18th Oil Shale Symposium.

(5) Forsman, J. P. and J. M. Hunt, Geochem. et Cosmochim. Acta, V. 15, pp. 170-182, 1958.

(6) Smith, J. W., U.S. Bureau of Mines, Report of Investigations 5725, 1961.

(7) Stanfield, K. E., I. C. Frost, W. S. McAuley and N. H. Smith, U.S. Bureau of Mines Rept. of Investigations, 4825, 1951.

(8) Giauque, R. D., J. P. Fox, and J. W. Smith, Lawrence Berkeley National Laboratory Report LBL-10809 UC-91, 1980.

(9) Singleton, M. F., G. J. Koskinas, A. K. Burnham, and J. H. Raley, Lawrence Livermore National Laboratory Report UCRL-53273, 1982.

(10) Copper, J. E. and W. S. Evans, Science, V. 219, pp. 492-493, 1983.

(11) Nadkarni, R. A., ACS, Symposium on Chemistry and Geochemistry of Oil Shales, Seattle, Wash., March 20-25, Preprints, V. 28, No. 3, pp. 200-208, 1983.

(12) Loughnan, F. C. and F. Ivor Roberts, Min. Mag. V. 47, pp. 327-334, 1983.

(13) White, J. S., Associate Curator-in-Charge, Division of Mineralogy, U.S. National Museum of Natural History, Smithsonian Institution, provided us with a sample of buddingtonite. The sample is identified as "California 117751-6. Received 1983.

(14) Young, N. B., J. W. Smith and W. A. Robb, Report of Investigations 8008, Laramie Energy Research Center, Laramie, Wyo., 1975.

(15) Sandholtz, W. A., Raley, J. H., Galloway, T. R., Rothman, A. J., Biermann, A. H., and G. S. Smith. Lawrence Livermore National Laboratory, Report UCID-19261, 1981.

(16) Stout, N. D., G. J. Koskinas and S. Santor, Lawrence Livermore National Laboratory, Report UCRL-52158, November 1976.

(17) Bremner, J. M., in Methods of Soil Analysis, Part 2, edited by C. A., Black, American Society of Agronomy, Inc., Publisher, Madison, Wisconsin, 1965.

(18) Vadovic, C. J., ACS, Symposium on Chemistry and Geochemistry of Oil Shale, Seattle, Wash., March 20-25, V. 28, No. 3, pp. 148-157 (1983).

(19) Robl, T. L., Project Coordinator, Resource Assessment of Oil-Bearing Shales in Lewis and Fleming Counties, Kentucky, V.II Supporting Data, IMMR 80/D-19/2b, 1980.

(19) Rubel, A. M., D. W. Koppenaal, D.N. Taulbee and T. L. Robl, 16th Oil Shale Symposium, Proceedings, p132, Colorado School of Mines Press, Golden Colorado, 1983.

(20) Baughman, G. L., Compiler, Synthetic Fuels, Data Handbook, Second Edition, p. 134, Cameron Engineers, Inc., 1315 South Clarkson Street, Denver, Colorado, 80210, 1978.

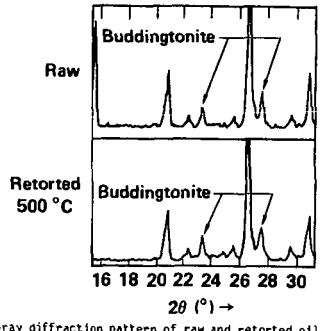

Figure 1. X-ray diffraction pattern of raw and retorted oil shale sample RI 8008-76 in which buddingtonite is found. Retorting does not eliminate the lines due to buddingtonite. The large peak on the left side of the raw-shale pattern is due to dawsonite. This mineral is decomposed during retorting.

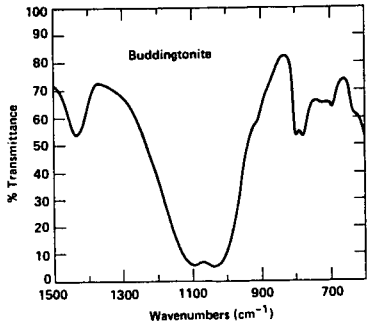

Figure 2. Infrared adsorption of buddingtonite showing the 1430 cm^{-1} peak due to ammonium ions. Sample from the Smithsonian Institute (SI), White (13).

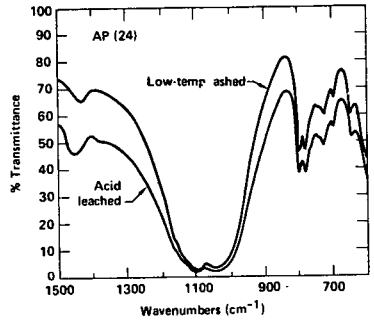

Figure 3. Change of infrared adsorption AP(24) shale. Lower curve acid leached shale and upper curve acid leached and low-temp ashed.

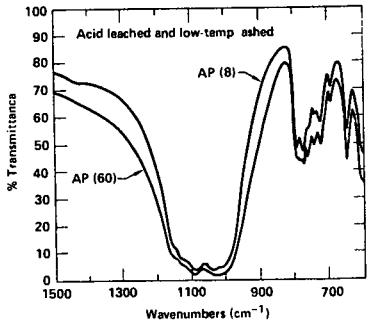

Figure 4. Infrared absorption of shales AP(60) and AP(8) which have been acid leached and low-temperature ashed. Shale AP(8) shows some ammonium-ion absorption and shale AP(60) does not.

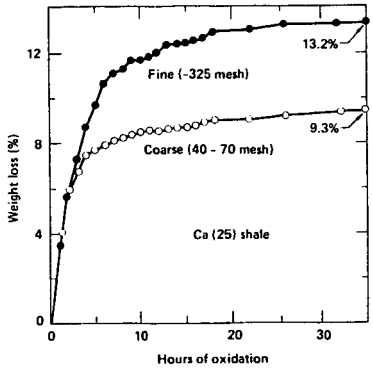

Figure 5. Weight loss during low-temperature ashing of raw shale Ca(25). The samples were stirred at the time of each data point.

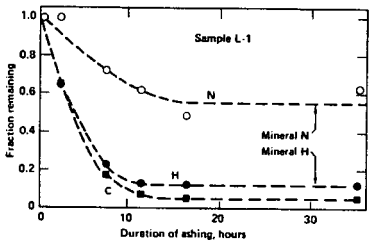

Figure 6. Fractional loss of N, H, and C during low-temperature ashing of sample L-1(9A/5). Residual N and H is due to the presence of these elements in minerals.

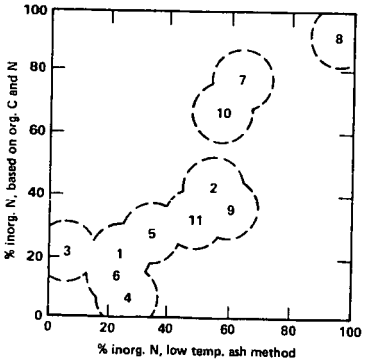

Figure 7. Comparison of inorg. N content of 11 shale samples as determined by two methods.

Naturally Occurring Arsenic Compounds in a Green River Oil Shale

James Jaganathan, Mysore S. Mohan and Ralph A. Zingaro

Department of Chemistry and the Coal and
Lignite Research Laboratory
Texas A&M University
College Station, Texas 77843 U.S.A.

The distribution of arsenic among the various components of a sample of Green River oil shale has been investigated. A number of arsenic species, some of which have not been previously reported, have been identified. The greatest fraction of arsenic, 65 percent of the total, was found to be present as skutterudite, (Co, Fe, Ni)As_3 and safflorite, (Fe, Co)As_2. About 16 percent was present in an HCl-soluble fraction, very probably in the form of arsenate. Almost nine percent was extracted by HF with the quartz and silicates. The bitumens and kerogens accounted for three and four percent of the total As, respectively, and this was found to exist in the form of methylarsenic and dimethylarsenic compounds. No evidence was found for the residence of arsenic in the pyrite.

Among the fossil fuels, oil shales are known to have the highest concentrations of arsenic, averaging 44 ppm. During recent years, and at the present time, there has existed a great deal of public concern about the contamination of the environment. Also, the refining of shale oils will utilize catalysts which are widely used in petroleum technology, viz., platinum and palladium. Arsenic is well-known to act as a poison toward such catalysts. Primarily for these two reasons information about the modes of occurrence of arsenic in oil shales is of importance.

Fish and co-workers (1) using a high performance liquid chromatograph coupled to a graphite furnace atomic absorption detector were able to confirm the presence of methylarsonic acid, benzenearsonic acid and arsenate in oil shale retort and process waters. Fish and Brinckman (2) studied the methanol extracts obtained from Green River oil shales. They reported the presence of the same three arsenic species in such extracts and the presence of other unidentified organoarsenic compounds. Jeong and Montagna (3) performed a gravitational separation followed by an isodynamic magnetic separation of pulverized Green River oil shale. Based on the enrichment of arsenic in fractions with higher magnetic susceptibility, they concluded that there exists an association between the arsenic content and iron-containing sulfide minerals such as $Fe_{1-x}S$ and $Fe(AsS)_2$.

In this report we describe the results of a systematic study of the distribution of arsenic among the various components which constitute a sample of Green River oil shale. Of the total arsenic, 97 percent was accounted for. The most significant result was the discovery of the presence of two arsenic minerals which account for two thirds of the total arsenic. These had not been previously found in oil shales.

EXPERIMENTAL

The oil shale sample used in this study was from the Hell's Hole Canyon of northeast Utah which forms part of the Uinta basin (Mahogany Zone). The sample, after it was disaggregated with a "Shatterbox" and screened through a U.S. standard -100 mesh sieve, had the following proximate analysis:

% moisture, 0.26±0.02; % volatiles, 41.89±0.14; % ash, 57.92±0.24; fixed carbon (by difference), 0.18±0.12.

Metal Analyses. Arsenic and iron in aqueous solutions were determined using a Perkin-Elmer Model 272 graphite furnace atomic absorption spectrometer. Nickel, at a concentration of 400 ppm was added as a matrix modifier in the arsenic analyses. Corroboration of the As and Fe values and the determinations of the other metal ion concentrations were performed with an ARL Model 34000, simultaneous, vacuum inductively coupled argon plasma emission spectrometer (ICPAES).

Ashing. A Branson/IPC, Model 4005-448 AN Automated Radio Frequency Plasma Asher was used to prepare the low temperature ash from the raw shale and the residue obtained following each acid demineralization step (Figure 1).

Arsenic Speciation. Arsenate, arsenite, methylarsonic and dimethylarsinic species were converted to the hydrides which separated and analyzed for separately. Details of the method are described elsewhere (4, 5). The technique, in addition to being very sensitive, makes possible a differentiation between inorganic As(III) (reduction by BH_4^- at pH 6.5) and inorganic As(V)(both As(III) and As(V) are reduced at pH 2). Methylarsenic and dimethylarsenic compounds are reduced to $MeAsH_2$ and Me_2AsH, resp. These are trapped at liquid nitrogen temperatures and easily separated by fractional distillation. Control experiments using $MeAs(O)(OH)_2$ and $Me_2As(O)OH$ showed that the conditions used for digestion of the kerogens and bitumens, viz., concentrated nitric acid at temperatures not exceeding 100°C for 2 h in a capped flask followed by the addition of 1 ml. of $HClO_4$ (70 percent) at the same temperature for 30 min., does not cause any rupture of H_3C-As or H_3C-As-CH_3 bonds. Known compounds were converted quantitatively to the arsines following this treatment.

X-Ray Diffraction and SEM-EDS Measurements. Diffractograms of the minerals in the low temperature ash samples, of the raw oil shale and of the residues remaining after successive demineralization treatments were obtained with the use of a Seifert-Scintag PAD II powder diffractometer automated by a DGC Nova 3 computer.

Scanning electron microscopy with energy-dispersive X-ray spectrometric measurements were carried out at the Electron Microscopy Center, Texas A&M University. The instrument used was a JEOL 35CF electron microscope equipped with energy-dispersive and wavelength dispersive spectrometric capabilities, digital beam control and dual wavelength capability.

RESULTS AND DISCUSSION

Figure 1 outlines a flow diagram which describes the chemical separation sequences used in this study. Powder X-ray diffraction studies revealed the presence of minerals typical of Green River oil shales with albite ($NaAlSi_3O_8$), dolomite ($CaCO_3 \cdot MgCO_3$) and quartz comprising the major mineral phases. Other minerals which were identified and found to be present in significant concentrations were pyrite (FeS_2), orthoclase ($KAlSi_3O_8$) and calcite.

Studies of the X-ray powder patterns at various stages of demineralization showed that treatment with 5M HCl was accompanied by the removal of dolomite and calcite. In the HCl-HF treated shale only pyrites appear to remain. The intensities of their characteristic spacings appear to be enhanced, probably due to the removal of other minerals. As expected, following treatment with HNO_3, the pyrite peaks disappear. The matter remaining at the end of the successive acid treatments was characterized by the absence of diffraction peaks. This is attributed to the amorphous and micro-crystalline nature of the material.

In Table 1 are listed the concentrations of arsenic and iron in various oil shale components separated according to the Scheme in Fig. 1. The results show that the bulk of the arsenic, ∿65 percent of the total, can be extracted by 2M nitric acid. Sixty percent of the iron is also extracted by this reagent.

Identification of Skutterudite and Safflorite. Fragments of the shale were fractured from a large 10 kg sample. Based on visual observation, the fragments collected represented both darker (presumably oil-rich) and lighter layers. The fragments collected were examined as follows: 1. The fragments were embedded in thermoplastic cement (Buehler Sci. Co., Cat. No. 40-8100); 2. the mounted samples were polished with alumina to a grit of 0.3μ. 3. in the case of some fragments originating from the more lightly colored layers of the shale sample, lustrous, silver grey mineral particles became visible. 4. the prepared samples were coated with 25Å thick layer of carbon and examined by SEM-EDS. 5. based on the x-ray microanalysis, large (1∿2 mm) mineral particles of interest were extracted from the SEM speciments after dissolving the cement with acetone; 6. x-ray powder diffractograms were obtained of these particles and, following their dissolution in HNO_3, metal ion concentrations were determined by ICPAES.

Figure 2 shows the electron micrograph of an arsenic-containing mineral particle and the energy-dispersive x-ray spectrum of the same particle. Several spot analyses on the silver-grey mineral grain indicated, based on a standardless semi-quantitative procedure (SSQ), the following uniform composition: %As, 76.7; %Fe, 8.90; %Co, 10.2, %Ni, 4.1. There was no evidence of the presence of sulfur in these particles. Evidence that these particles were composed of skutterudite and safflorite was obtained from measurements of the d-spacings in their x-ray powder diffractograms as is illustrated in Fig. 3. Further corroboration was obtained from the results of analytical measurements (ICPAES) of the metal ion content of these particles: %As, 71.4; %Fe, 10.4; %Co, 3.9; %Ni, 5.1; %Ca, 4.2. The composition of the arsenide minerals excluding calcium was as follows: %As, 74.6; %Fe, 10.8; %Co, 9.3; %Ni, 5.3 giving a stoichiometry of $Fe_{1.0}Co_{0.82}Ni_{0.46}As_{5.1}$.

Examination of about seventy pyrite particles, by SEM-EDS, with x-ray photons being accumulated, in some cases, for periods as long as 5000 seconds, showed no evidence of the presence of arsenic. These results indicated quite conclusively that in this oil shale sample the arsenic is present as skutterudite, $(Co,Fe,Ni)As_3$ and safflorite, $(Fe,Co)As_2$, but not with pyrite.

Methylated Arsenic Compounds in Bitumen and Kerogen. Samples of bitumen and kerogen were analyzed for total arsenic by digestion with con HNO_3 followed by con $HClO_4$ and taken to fuming. They were also analyzed by hydride reduction techniques following digestion methods which keep the H_3CAs and $(H_3C)_2As$ bonds in tact (see exptl. part). The results of these studies show very clearly that only a minor fraction of the total arsenic in these organic components is present in the form inorganic arsenic(V). This is possibly due to the distribution of small quantities inorganic arsenic minerals with these components. The bulk of the arsenic in both the bitumens and kerogens is present as H_3C-As and$(H_3C)_2As$ species. These results have not yet been quantitated.

CONCLUSION

The bulk of the arsenic in a sample of Green River oil shale, almost 65 percent of the total, is present as skutterudite and safflorite.

None was found to be associated with the pyrites. About 16 percent of the arsenic is extracted by HCl, and this may be in the form of arsenates. The HF-solubles, primarily quartz and silicates, have about nine percent of the total arsenic. The bitumens and kerogens accounted for three and four percent of the

total original arsenic and this was found to contain significant amounts of methyl and dimethylarsenic compounds.

ACKNOWLEDGEMENTS

We wish to thank the Center for Energy and Mineral Resources of Texas A&M University and the Robert A. Welch Foundation of Houston, Texas, for financial assistance in support of this work. Mr. James Ehrman, the Electron Microscopy Laboratory of Texas A&M University furnished invaluable advice and assistance in acquiring and interpreting the SEM-EDS data.

REFERENCES

1. Fish, R.G., Brinckman, F.E. and Jewett, K.L., Environ. Sci. Technol., 16, 174 (1982).

2. Fish, R.H., Brinckman, F.E., Preprints ACS Div. of Fuel Chem., 28, No.3, 177 (1983).

3. Jeong, K.M. and Montagna, J.C., Preprints ACS Div. of Fuel Chem., 29, No.3, 307 (1984).

4. Mohan, M.S., Zingaro, R.A., Micks, P. and Clark, P.J., Intern. J. Environ. Anal. Chem., 11, 175 (1982).

5. Clark, P.J., Zingaro, R.A. Irgolic, K.J. and McGinley, A.N., Intern. J. Environ. Anal. Chem., 7, 295 (1980).

Table 1. Distribution of Arsenic and Iron among Oil Shale Components*

Sample description	As μg/g oil shale		Iron g/100 g oil shale	
	GF-AAS	ICPAES	GF-AAS	ICPAES
Raw shale	72.3±0.68	68±1.2	2.23±0.02	2.24±0.01
HCl-soluble	13±0.1	10±0.1	0.49±0.003	0.47±0.004
HF-soluble	6.34±0.06	------	0.35±0.004	------
HNO_3-soluble	46±0.6	47±0.4	1.34±0.03	1.31±0.03
THF-soluble	1.88±0.11	2.12	------	------
R**	3.28±0.02	3.23±0.01	------	------

*Each value represents an average of the results of at least three experiments.
** R: HCl-HF-THF-HNO_3-treated oil shale.

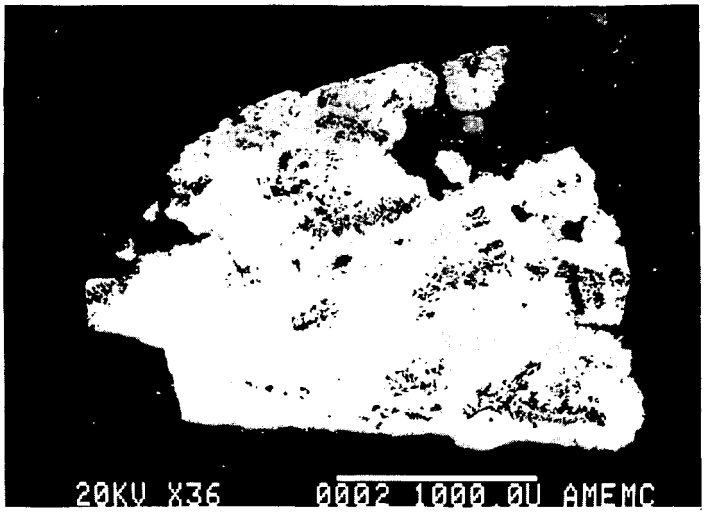

Fig. 2a. Electron micrograph of arsenic-rich mineral, magnification x36.

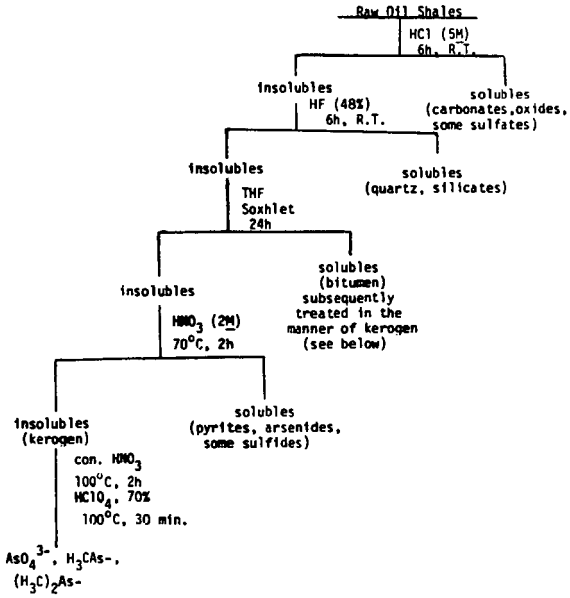

Fig. 1. Flow Diagram of the Sequence of Chemical Separation of Oil Shale Components.

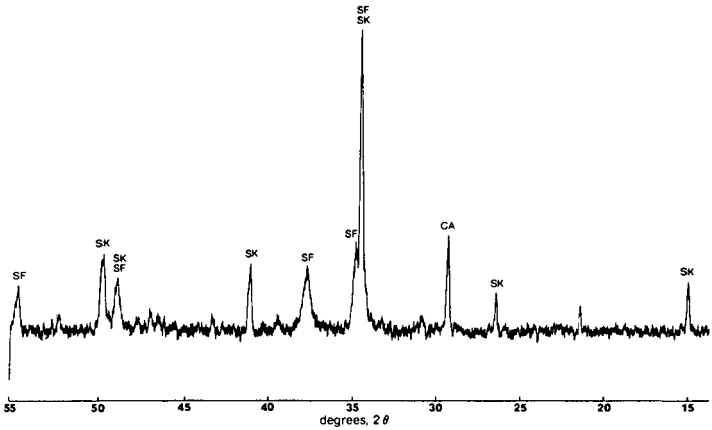

Fig. 3. Powder x-ray diffractogram of the particle in Fig. 2a. Key to symbols: SK, skutterudite; SA, Safflorite; CA, calcite.

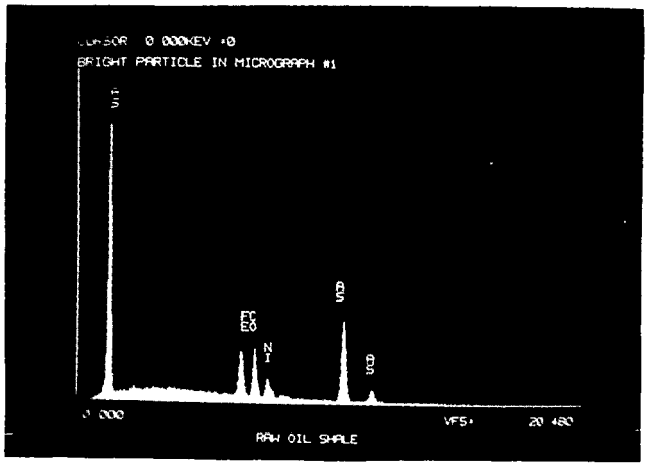

Fig. 2b. Energy-dispersive x-ray spectrum of the particle in Fig. 2a.

Effect of Acid-Clay Treatment on Nitrogen Compound Distribution in Fuels from Shale Oil

Steven A. Holmes and William E. Blanton

Western Research Institute
P. O. Box 3395, University Station
Laramie, Wyoming 82071

INTRODUCTION

The properties of fuels have been studied extensively in relation to the effects of processing on them and their effect on thermal and/or storage instability. Studies indicate nitrogen species in hydrotreated fuels derived from shale oil have deleterious effects on fuel stability (1). The speciation of nitrogen compounds at ppm levels in fuel provides information regarding fuel stability and allows possible selection of antioxidant additives. However, little information is available regarding speciation of nitrogen compounds at trace levels in fuels.

Comparing physicochemical properties of an oil before and after processing has provided insight to processing effects. Nitrogen compound-type distributions in crude shale oil and in fuels produced by catalytic hydrotreatment have been studied (2,3). Catalyst selectivity toward hydrodenitrogenation of different nitrogen types has been determined. Other oil-upgrading schemes have incorporated acid treatment of shale oils (4). In 1979, Standard Oil of Ohio (Sohio) hydrotreated shale oil to remove 80 percent of its nitrogen; however, about 3350 ppm nitrogen remained in the hydrotreated products (5). These products were subsequently treated with acid and clay to remove residual fuel-bound nitrogen and color bodies, making the finished products storage stable. Finished jet fuel contained less than one ppm nitrogen, and finished diesel fuel contained 23 ppm nitrogen. Sohio reported that acid-clay treatment also removed non-nitrogen containing compounds.

With the development of high resolution gas chromatographic capillary columns and computer data base reduction systems, analytical techniques have allowed efficient speciation of nitrogen compounds in fuels (6). The following work presents the speciation of nitrogen compounds in hydrotreated and finished fuels derived from shale. A comparison of these compound types is used to discuss effects of acid-clay treatment of the fuels. An analysis of the nitrogen types in the finished fuel is discussed in terms of their reactivity toward fuel instability.

EXPERIMENTAL

Hydroprocessing of Shale Oil

Shale oil from the Paraho direct heat retort was hydroprocessed by Sohio under a contract with the U.S. Departments of Energy and Defense (5). Whole crude oil was catalytically hydrotreated over a nickel-molydenum catalyst and then fractionated by distillation to maximize yields of military transportation fuels, jet fuels (JP-5 and JP-8) and diesel fuel marine (DFM). Each hydrotreated fuel was treated with acid and clay. About 10.8 kg of 93 weight percent sulfuric acid was used to contact each bbl of fuel; the acid-treated fuel was separated from the acid sludge and passed through clay filters, a clay contactor, and final filter to product storage. An antioxidant was added to the acid-clay treated fuel. The effect of acid-clay treatment on nitrogen compound-type distribution was investigated by analyzing the compositions of the hydrotreated DFM and the finished DFM.

Fractionation by Adsorption Chromatography

Preparative alumina adsorption chromatography was used to fractionate the hydrotreated DFM and finished DFM into hydrocarbon and nitrogen fractions. An accurately weighed amount of hydrotreated DFM (about 10 grams) was diluted with 100 ml of hexane and pumped onto basic alumina in a 0.9 cm i.d. x 50 cm glass column. An additional 100 ml of hexane eluted the hydrocarbon fraction from basic alumina. The nitrogen fraction was backflushed from the column with 40 volume percent ethanol in toluene. Because some nitrogen compounds remained in the hydrocarbon fraction, this fraction was chromatographed again on neutral alumina into hydrocarbon and pyridine fractions. An accurately weighed amount of the finished DFM (about 174 grams) was diluted with 1800 ml hexane and pumped onto neutral alumina. An additional 100 ml of hexane eluted the hydrocarbon fraction from the column and the nitrogen fraction was backflushed from the neutral alumina with 40 volume percent methanol in benzene. Rates for sample charging and fraction elution were 6 ml/min. Solvents were carefully removed from fractions under reduced pressure. Solvent-free fractions were weighed and stored under nitrogen in refrigerated amber glass containers until compound-type analyses.

Analytical Methods

Elemental nitrogen in the fuels and their fractions was determined by chemiluminescence detection. Standard solutions ranging from 3×10^{-2} M to 5×10^{-5} M 9-methylcarbazole in toluene were used as calibrants. Amounts of basic nitrogen were determined by potentiometric titration analysis using acetonitrile-toluene and acetic anhydride-toluene with perchloric acid in dioxane as titrant (3). These reported values are accurate within ±3 relative percent. Infrared spectra were obtained with a Perkin-Elmer model 621 grating spectrophotometer. The nitrogen-containing fractions were diluted in methylene chloride, and spectra recorded in the absorbance mode using solvent compensation with a matched pair of potassium chloride infrared cells of path length 0.5 mm.

High resolution gas chromatographic analysis (HRGC) of the nitrogen-containing fractions was done with an HP model 5730A equipped with a capillary column inlet system. A 60-meter DB-1 fused silica capillary column was used with a glass effluent splitter (1:1) for simultaneous flame ionization (FID) and nitrogen-phosphorous detection (NPD). Helium was used as carrier gas. Column linear flow velocity was 20 cm/sec. Samples were diluted with methylene chloride, and splitless injections having a 45-second delay time were used with a 30°C initial oven temperature for the nitrogen-containing fractions from the hydrotreated DFM. A 140°C initial oven temperature was used for the nitrogen fraction from the finished DFM. Oven temperature was programmed to 300°C at 2°C/min.

Similar gas chromatographic conditions described above were employed for compound-type analysis by high resolution gas chromatography/mass spectrometry (HRGC/-MS). An upgraded HP model 5985 was used with an interface temperature of 300°C. Source temperature was 200°C, and ionization voltage was 70V. A mass range from 45 to 500 amu was scanned.

RESULTS AND DISCUSSION

Concentration of Nitrogen Compounds by Chromatography

The nitrogen compounds in the fuels were concentrated to facilitate detailed compound-type characterization. Two nitrogen-containing fractions from the hydrotreated DFM and one nitrogen fraction from the finished DFM were generated by alumina adsorption chromatography. A pyridine fraction from the hydrotreated DFM was identified by its distinct infrared absorbances at 1598 cm^{-1} (C=C stretch) and 1557 cm^{-1} (C=N stretch), suggesting the presence of pyridinic compounds. The absence of these absorbances in the finished DFM confirmed the lack of a pyridine fraction

as well as pyridinic compounds. The nitrogen fractions from both fuels displayed N-H stretching at 3460 cm^{-1}, suggesting the presence of pyrrolic compounds.

Nitrogen compounds comprised 6 weight percent and 0.13 weight percent of the hydrotreated DFM and finished DFM (Table 1), respectively. The low nitrogen contents in the pyridine fraction (2.92 weight percent) and in the nitrogen fraction from the finished DFM (1.62 weight percent) suggest the presence of non-nitrogen containing compounds. However, excellent nitrogen recovery was obtained. About 99 percent and 91 percent of the nitrogen from the hydrotreated DFM and finished DFM, respectively, was concentrated in the pyridine and nitrogen fractions.

Amounts of basic nitrogen were determined in each of the nitrogen-containing fractions and are presented in Table 2. All the nitrogen in the pyridine fraction was weak base (pka 7 to 9), suggesting the presence of pyridine derivatives. The potentiometric titration analysis of the nitrogen fraction from the hydrotreated DFM indicates not only pyridinic compounds but also the presence of arylamines and hydrogenated indoles and/or quinolines (pka 2 to 7), and indoles and carbazoles (nonbasic nitrogen). The nitrogen fraction from the finished DFM contains predominately nonbasic nitrogen which does not undergo extensive acetylation (27 percent) in acetic anhydride; this suggests the presence of nonactive hydrogens in indole- and/or carbazole-type compounds.

HRGC/FID/NPD and HRGC/MS Analysis

HRGC with simultaneous detection by FID and NPD was used to establish optimal gas chromatographic conditions for the HRGC/MS analysis presented below. Acceptable peak resolution without tailing was achieved on the apolar chromatographic column. In Figure 1, the one-to-one peak correspondence of each detector response to the components in the nitrogen fraction from the hydrotreated DFM suggests that this fraction contains compounds with at least one nitrogen atom. Phosphorous is not expected to be present in these fractions. However, in Figure 2 the FID/NPD responses of the species from the finished DFM indicate few nitrogen compounds which have long column retention times (initial oven temperature, 140°C). FID/NPD responses for species in the pyridine fraction indicate the presence of non-nitrogen-containing compounds. The nitrogen species in the pyridine fraction are distributed about intermediate column retention times compared with the longer times for species in the nitrogen fractions.

Nitrogen in the pyridine fraction is primarily found in the isomers of alkyl-substituted dihydropyridines, pyridines, quinolines, and tetrahydroquinolines shown in Table 3. It is noteworthy that many different isomers of alkyltetrahydroquinolines are indicated relative to fewer alkylquinolines. The buildup of tetrahydroquinolines is indicative of the rate determining step in the hydrogenation of quinoline. The large number of isomers of alkylpyridines has been observed previously (7). Not listed for the pyridine fraction are non-nitrogen-containing compounds which include alkyl-substituted benzenes, naphthenes, biphenyls, and 9-H fluorenes. Because compound-type sensitivity factors were not available at the time of analysis, quantitative data were not obtained.

Large numbers of isomers of alkyltetrahydroquinolines and alkylpyridines are indicated by HRGC/MS analysis of the nitrogen fraction from hydrotreated DFM. These results are listed in Table 3. Infrared absorbances at 3375 cm^{-1} (N-H stretch) and 1612 cm^{-1} and potentiometric titration analysis (pka 2 to 7) suggest that arylamines are also in this fraction. Because chemical ionization was not done, analysis by electron impact ionization cannot differentiate arylamines from pyridines. Previous work (8) showed about 15 percent of the pyridines may be comprised of arylamines. In addition, alkyl-substituted pyrroles, indoles, and carbazoles are present.

The retention time of carbazole in the total ion current chromatogram (TICC) of the nitrogen fraction from the hydrotreated DFM is indicated in Figure 3. The ex-

tracted ion current profiles (EICP) of methylcarbazoles and dimethylcarbazoles are shown in Figure 4. These compound types have long column retention times, and they comprise minor amounts of nitrogen in the fuel as indicated by their ion intensities.

The HRGC/MS analysis of the nitrogen fraction from the finished DFM was facilitated by matching its FID/NPD chromatograms (Figure 2) with that of its TICC. Mass spectral fragmentation patterns of the few nitrogen-containing compounds in this fraction are tentatively identified as carbazole, methylcarbazoles, and dimethylcarbazoles. Except for the ion intensity of carbazole in the finished DFM, relative intensities of the alkylcarbazoles in the finished DFM agree very well with those in the hydrotreated DFM. No other nitrogen types were identified; however, this does not preclude minor amounts undetected at baseline levels. The non-nitrogen-containing compounds were alkyl-substituted naphthalenes and 9-H fluorenes.

Effect of Acid-Clay Treatment on Nitrogen Compound Distribution

A comparison of the nitrogen compound distributions in fuels before and after acid-clay treatment demonstrates which nitrogen types are susceptible to removal. Acid-clay effectively removed 99.3% of the nitrogen from the hydrotreated DFM. As expected, basic nitrogen compounds such as arylamines form salts in reaction with acid; pyridine derivatives adsorb into acidic medium and/or participate in electrophilic substitution reactions, and both compound types are removed as acid sludge. A pyridine fraction was present only in the hydrotreated fuel and was completely removed by the acid-clay treatment. Very weak base and nonbasic nitrogen compounds such as indoles, which experience adsorption and/or acid catalysis and polymerization reactions, are effectively removed by acid-clay treatment. Interestingly, some carbazole derivatives survive acid-clay treatment. Earlier work (8) showed carbazole derivatives constituted about 66 ppm nitrogen in the hydrotreated DFM. Therefore, acid-clay removed almost two-thirds of the carbazole derivatives from the hydrotreated DFM. Nonbasic carbazoles are soluble in mineral acids; their relative unreactivity allows some to remain in the finished fuel.

In the acid-clay treatment of jet fuel (JP-8), nitrogen was not detected in the finished fuel. High resolution mass spectrometric analysis of the hydrotreated JP-8, which contained 3000 ppm nitrogen, indicated similar nitrogen-type distribution to that in the hydrotreated DFM, except carbazole derivatives were not detected. Acid and clay effectively removed all nitrogen types from the JP-8 fuel. Carbazole derivatives in transportation fuels are the nitrogen compounds least affected by acid-clay treatment.

The importance of determining residual nitrogen types in finished fuels relates to fuel stability. Aromatic nitrogen compounds have measurable sediment under low temperature storage conditions. Work reported (9) on model compounds has indicated that symmetrical, highly condensed aromatic nitrogen compounds appear less reactive than the partially hydrogenated counterparts or highly alkylated heterocyclics. These model compound studies suggest carbazole derivatives do not participate as significantly in sediment formation as do pyrrole and indole derivatives. Synergestic effects also play an important role in sediment formation particularly as the hydrocarbon matrix becomes more complex: n-decane<jet fuel<diesel fuel. The nitrogen distributions in the finished DFM and JP-8 fuels indicate these fuels may be storage stable. However, non-nitrogen compound types in these fuels may very well affect fuel stability.

In summary, the analytical techniques presented have been applied successfully to the analysis of moderate and trace quantities of nitrogen in fuels. The determination of nitrogen compound distributions aid in understanding the effects of fuel processing and in discussing fuel stability.

ACKNOWLEDGMENTS

The authors are indebted to E. T. Robinson of Sohio for discussions of this work. The authors thank the following personnel at WRI for their technical contributions: L. F. Thompson, F. A. Barbour, S-L Chong, and M. Harnsberger. They also thank R.E. Robertson for reviewing the manuscript and M. E. Marron for editorial suggestions.

LITERATURE CITED

1. Frankenfeld, J. W., W. F. Taylor, and D. W. Brinkman. Exxon R and E Co., U.S. Department of Energy Contract Report No. DOE/BC/10045-12 (1981).

2. Bett, A., T. G. Harney, T. W. Matheson, and K. C. Pratt. Fuel, 62, 1445 (1983).

3. Holmes, S. A. and L. F. Thompson. Preprints, Div. of Petrol. Chem., ACS, 29 (1), 269 (1984).

4. Reif, H. E., J. P. Schwedock, and A. Schneider. "An Exploratory Research and Development Program Leading to Specifications for Aviation Turbine Fuel From Whole Crude Shale Oil, Part V," Final Report AFWAL-TR-81-2087, March 1982. Available from NTIS.

5. Evin, C. G. and E. T. Robinson. "The Commercial-Scale Refining of Paraho Crude Shale Oil Into Military Fuels," Office of Naval Research, Navy Contract N0014-79-C-0061, Sept. 1979.

6. Ellis, L. C., and P. T. Crisp. J. Chrom., 292, 355 (1984).

7. Cooney, J. V., E. J. Beal, and R. N. Hazlett. Preprints, Div. of Petrol. Chem., ACS, 29 (1), 247 (1984).

8. Holmes, S. A., and L. F. Thompson. Fuel, 62, 709 (1983).

9. Frankenfeld, J. W., W. F. Taylor, and D. W. Brinkman. Exxon R and E Co., U.S. Department of Energy Contract Report No. DOE/BC/10045-23 (1982).

DISCLAIMER

Mention of specific brand names or models of equipment is for information only and does not imply endorsement.

Table 1. Nitrogen Content in Fractions from Fuels Derived from Shale

Fractions	Weight Percent Sample	Weight Percent Nitrogen	Nitrogen (Weight Percent of Sample)
Hydrotreated DFM			
Pyridine Fraction	1.46	2.92	0.043
Nitrogen Fraction	4.58	6.31	0.289
Hydrocarbon Fraction	91.5	11 ppm	10 ppm
Recovery (%)	98	NA	99
Finished DFM			
Nitrogen Fraction	0.13	1.62	21 ppm
Hydrocarbon Fraction	94.2	2 ppm	2 ppm
Recovery (%)	94	NA	100

Table 2. Distribution of Basic Nitrogen Contents in Fractions from Fuels Derived from Shale

Fractions	Weight Percent of Nitrogen		
	Weak Base pka 7 to 9	Very Weak Base pka 2 to 7	Nonbasic Nitrogen
Hydrotreated DFM			
Pyridine Fraction	2.92	--	--
Nitrogen Fraction	4.78	0.76	0.77
Finished DFM			
Nitrogen Fraction	0.04	0.06	1.52

Table 3. Compound Classes in Fractions from Hydrotreated DFM

Compound Class[a]	No. of Isomers in Fraction		Compound Class	No. of Isomers in Fraction	
	Pyridine	Nitrogen		Pyridine	Nitrogen
Dihydropyridines			Quinolines		
C_7	6	--	C_0	--	1
C_8	4	--	C_1	--	1
C_9	4	--	C_2	1	2
Pyridines[b]			C_3	4	6
C_2	--	3	C_4	7	4
C_3	--	21	C_5	4	2
C_4	4	28	Indoles		
C_5	10	44	C_1	--	4
C_6	15	42	C_2	--	5
C_7	29	33	C_3	--	8
C_8	24	21	C_4	--	16
C_9	30	26	C_5	--	18
C_{10}	19	39	C_6	--	24
C_{11}	21	33	C_7	--	18
C_{12}	17	11	C_8	--	2
C_{13}	9	2	Pyrrole		
C_{14}	2	--	C_{10}	--	1
Tetrahydroquinolines			Carbazoles		
C_1	--	11	C_0	--	1
C_2	--	19	C_1	--	3
C_3	3	30	C_2	--	1
C_4	11	22	Acridines/		
C_5	13	37	Phenanthridines/		
C_6	9	28	Benzoquinolines	2	--
C_7	2	13			
C_8	1	--			

[a] Listing of C_x refers to the number of carbons in substituents on the heteroaromatic compound.

[b] Alkylarylamines are included with pyridines in the nitrogen fraction.

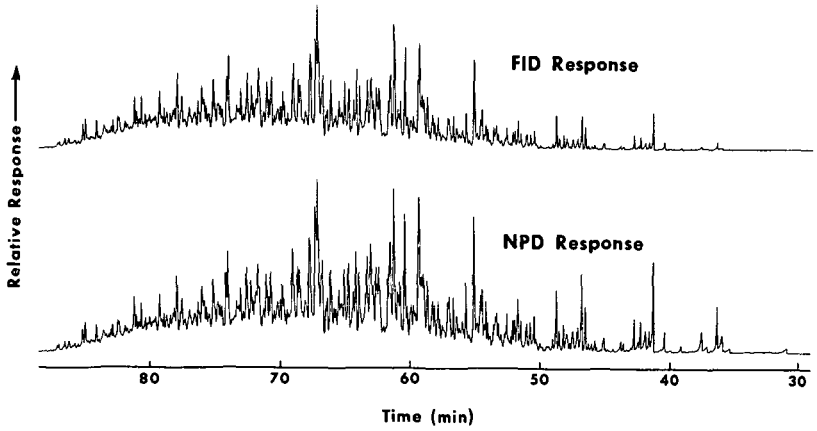

Figure 1. HRGC Chromatograms of Nitrogen Fraction from Hydrotreated DFM (Initial Oven Temperature, 30°C)

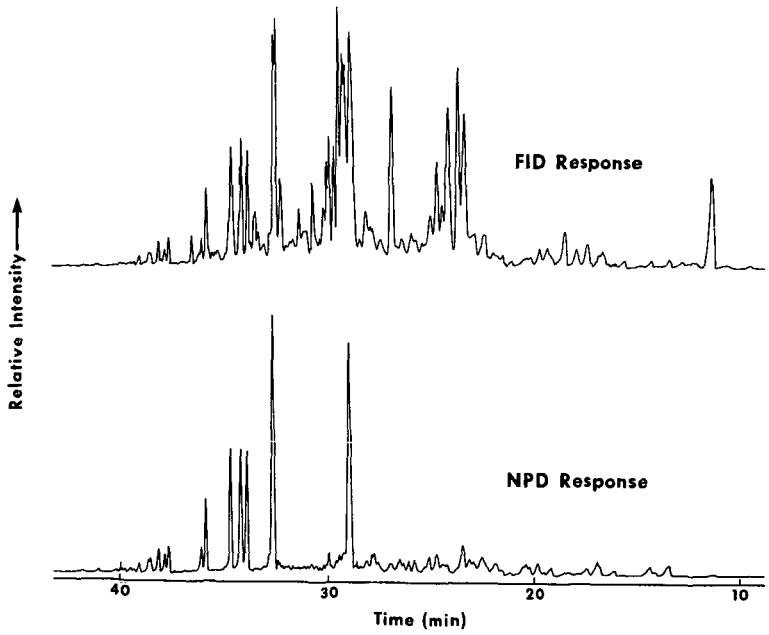

Figure 2. HRGC Chromatograms of Nitrogen Fraction from Finished DFM (Initial Oven Temperature, 140°C)

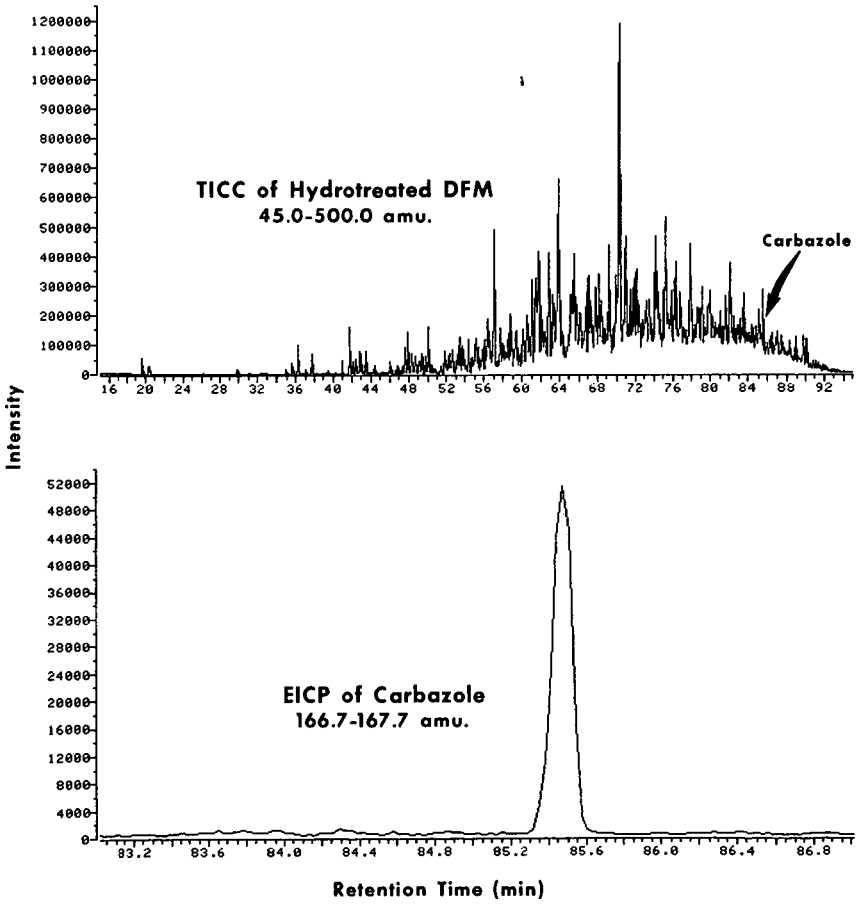

Figure 3. HRMS/GC Analysis of Hydrotreated DFM

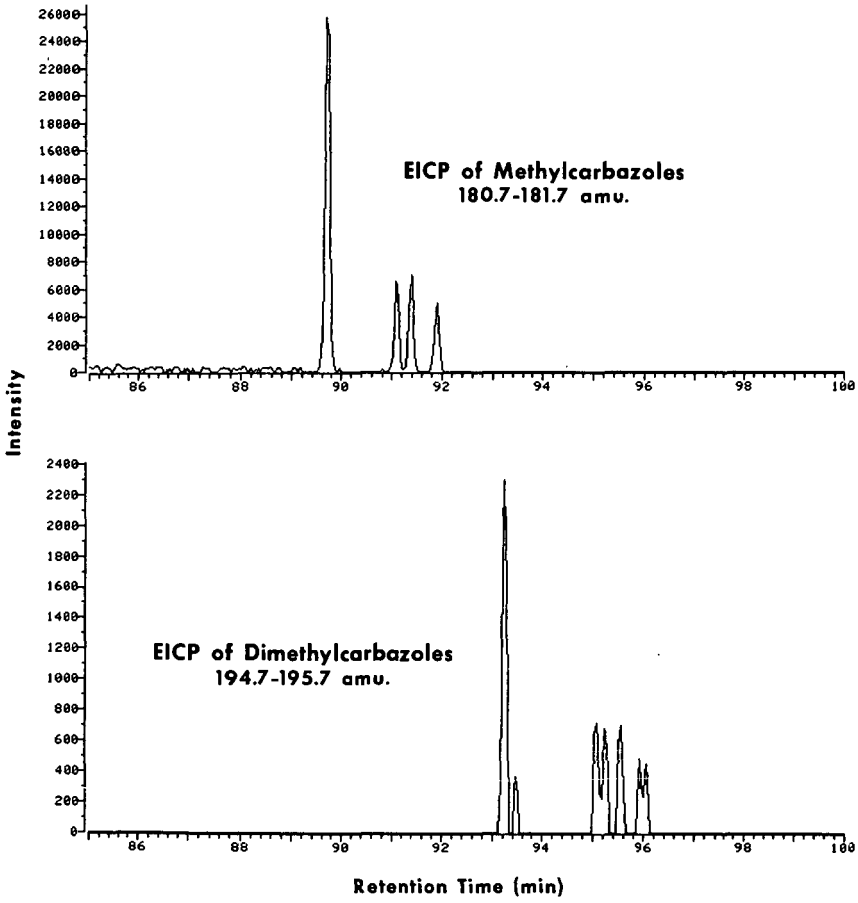

Figure 4. Extracted Ion Current Profile of Alkylcarbazoles